Journal of Pediatric Neurology 10 (2012) 87–94
DOI 10.3233/JPN-2012-0541
IOS Press

Impaired prefrontal cortical response by switching stimuli in autism spectrum disorders

Naoko Narita[a,*], Akiyuki Saotome[a], Hiroki Higuchi[a], Masaaki Narita[b], Mami Tazoe[c] and Kaoru Sakatani[d]
[a]*Institute of Education, Bunkyo University, Saitama, Japan*
[b]*Developmental and Regenerative Medicine, Mie University, Mie, Japan*
[c]*Department of Clinical Psychology, Japan Lutheran College, Tokyo, Japan*
[d]*Department of Neurological Surgery, Nihon University School of Medicine, Tokyo, Japan*

Received: 2 May 2011
Revised: 21 June 2011
Accepted: 27 June 2011

Abstract. Working memory (WM) performance is considered to change according to the nature of the task by adequate and prompt activation of corresponding functional connectivity in the brain. In the present study, we examined continuous prefrontal hemodynamic changes depending on reciprocal disposition of WM and non-WM tasks using two-channel near-infrared spectroscopy. To investigate possible functional connectivity deficits in autism spectrum disorder (ASD) during these tasks, relative concentration changes in oxygenated hemoglobin (Hb), deoxygenated Hb, and total Hb were compared between high-functioning ASD subjects (n = 11) and controls (n = 22). Instant evoked cerebral blood oxygenation changes were observed in response to the task switch in controls but not in ASD subjects, although the task performance rate was almost equivalent. Delayed or altered response of functional connectivity to incoming stimuli is considered a characteristic feature of ASD.

Keywords: Autism, executive function, working memory, default mode network

1. Introduction

Autism spectrum disorder (ASD) is a set of disorders associated with intercommunication and interrelation abilities that lead to impaired cognitive and emotional development [1,2]. Furthermore, functions of higher brain networks, such as theory of mind, central coherence, and executive functions are deficient to varying extents [3]. Although numerous studies on functional neuroimaging have been conducted [4–6], clear and consistent interpretation of the defects in the prefrontal cortex (PFC) and its signal processing have not been well understood until date.

*Correspondence: Dr. Naoko Narita, Institute of Education, Bunkyo University, 3337 Minamiogishima, 343-8511, Koshigaya-City, Saitama, Japan. Tel.: +81 489 7488 11; Fax: +81 489 748 960; E-mail: nnarita@koshigaya.bunkyo.ac.jp.

Working memory (WM) is an executive function related not only to brief information retention but also to information manipulation for problem solving, planning, and language processing [7]. Advanced neuroimaging studies involving healthy individuals have shown that the dorsolateral PFC (DLPFC) and multiple other brain regions are activated during WM functioning [8–10]. On the other hand, with ASD subjects results have been inconsistent and appear to depend largely on the nature of the task and profile. Some studies have reported certain deficits of spatial WM in ASD [11–13], while others lack evidence of inferior WM performance in ASD subjects compared to that in controls [14–16]. However, studies using functional magnetic resonance imaging (fMRI) almost invariably encountered lower DLPFC activation in ASD subjects than in controls, regardless of the task

performance rate [17,18]. This behavioral-neurofunctional discrepancy may be partially explained by a functional connectivity point of view. Functional connectivity techniques help us understand how brain regions contribute to functionally connect simultaneous circuits during a task [19].

Functional connectivity is generally systematically controlled. During the resting state, a network, including the medial PFC, is activated as a default mode network (DMN). When external cognitive demanding stimuli are received the dorsal attention network, including DLPFC is activated instead of DMN being deactivated [20]. DMN deactivation was found to be disrupted in ASD, which appears to coincide with DLPFC hypoactivation when compared to the resting state on fMRI [21,22].

Recently we used near-infrared spectroscopy (NIRS) to obtain numerous noninvasive measurements of regional cerebral blood oxygenation (CBO) in vivo [23–25]. This is advantageous because the portable nature of NIRS also enables reproduction of natural experimental conditions when providing continuous and repetitive stimuli to subjects [26,27].

We hypothesized that if ASD subjects have deficiencies in functional connectivity and appropriate activation-deactivation responses to incoming variable stimuli, continuous neurophysiological monitoring would reveal a delayed and/or defective response to frequent switching of tasks of a different nature. Therefore, in this study we used NIRS measurement of CBO in PFC during switching of WM and non-WM requiring repetitive stimulation and compared relative oxygenation changes in response to stimuli switches between ASD subjects and healthy controls.

2. Materials and methods

2.1. Participants

Eleven ASD subjects intelligence quotient (IQ) > 65 according to the Wechsler intelligence scale for children-III; aged 14–46 years (mean, 29.5 years); three males and eight females; (all right-handed) and 22 healthy controls aged 19–51 years (mean, 25.2 years); six males and 16 females; (20 right-handed; two left-handed) were examined. All subjects were diagnosed (Narita Naoko and Narita Masaaki) and assessed (Tazoe Mami) by pediatric neurologists and psychologists on the basis of developmental history and current presentation according to the diagnostic and statistical manual of mental disorders IV and the Japanese version of the autism diagnostic interview-revised. The study was approved by the research and ethics committee of Bunkyo University, and written informed consent was obtained from all subjects or their legal guardians prior to the study.

2.2. Methods

The task-switching paradigm was designed using randomized geometrical figures in combinations of three shapes (circle, triangle and square) and four colors (red, yellow, blue and green). The paradigm was originally constructed using commercial presentation software (PowerPoint 2003, Microsoft, USA) and was presented to the subjects using an automated slideshow on a personal computer (Fig. 1). For the tasks that required WM (WM task), the subjects were instructed to memorize figures that appeared one by one every 3 sec on the screen (WM stimuli) and to explore and touch the figures in consecutive order as memorized within the next 15 seconds from a multiple choice panel that appeared on the screen (WM exploration). For the tasks that did not require WM (NWM task), all test figures appeared at the same time in an inset together with multiple choices on the same screen. The subjects were instructed to explore and touch the figures in the correct order as they appeared in the inset by touching the screen within 15 sec (NWM exploration). For both tasks, the number of figures presented was increased in order from one to six (described as task 1, task 2, etc.), and the tasks were programmed and performed in WM-NWM order.

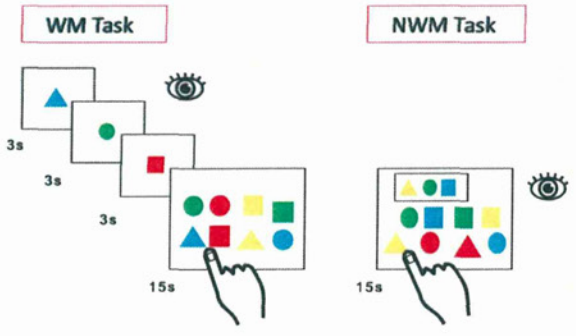

Fig. 1. An example illustration of the No. 3 task block of the experimental paradigm. After showing the subjects 3 geometrical shapes on the screen for 3 sec each (working memory [WM] stimuli), eight shapes are, shown for 15 sec and the subjects then search for and choose the shapes that they just memorized (WM exploration time). NWM exploration is, presented for 15 sec successively.

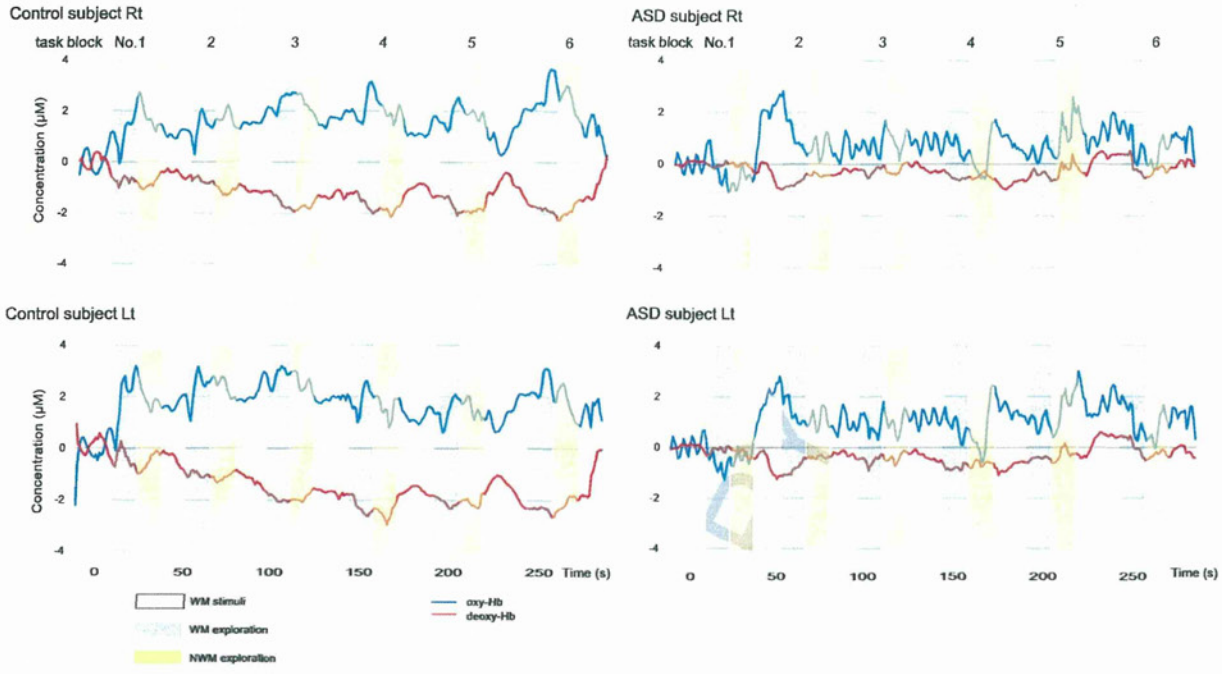

Fig. 2. Typical patterns of cerebral blood oxygenation changes measured by near-infrared spectroscopy in a control (46-year-old female subject) and an autism spectrum disorder patient (46-year-old female subject with high-functioning autistic syndrome). The right (top) and left (bottom) cerebral blood oxygenation changes in oxy-hemoglobin (blue lines) and deoxy-hemoglobin (red lines) are, indicated as relative values in units of μM. The periods of each task are color-coded. The numbers above indicate the task block number.

To facilitate calculation of task performance rate, we recorded the screen during the entire set of paradigm performances and the percentage of correct answers for each task was calculated after analyzing the tapes. The differences between WM and NWM tasks as well as between controls and ASD subjects were compared.

We measured evoked CBO changes using NIRO-200 (Hamamatsu Photonics K.K., Hamamatsu, Japan) as in our previous NIRS activation studies [27–29]. The sensors were placed symmetrically on the forehead and the midpoint between the two optodes was identical to the Fp2 position of the international electroencephalography 10/20 system [30]. Our previous MRI observations demonstrated that the emitter/detector should be placed over the frontal lobe, matching Brodmann's areas 8/9 of PFC [23], where near infrared light was and suspected to penetrate the depth of the cortical surface [31]. During performance of the switching task, concentration changes in oxygenated (oxy-) hemoglobin (Hb), deoxygenated (deoxy-) Hb, and total Hb were continuously measured with a time resolution of 1 sec.

For data analysis, baseline corrections were performed by subtracting an individual average baseline period from the value measured during each task. Then, the average Hb concentration in the 15-sec exploration periods during each task (WM and NWM) was calculated. Finally, relative value changes between corresponding WM and NWM exploration periods were evaluated by statistical analysis.

3. Results

Among the 11 ASD subjects, nine were diagnosed with Asperger syndrome and two with high-functioning autistic disorder. The mean full scale IQ was 99.4 (range 73–118), mean verbal IQ was 107.6 (89–120), and mean performance IQ was 89.5 (54–118) among ASD subjects according to Wechsler intelligence scale for children-III.

While recording NIRS data for a typical control subject, an increase in the oxy-Hb concentration was observed during the WM exploration period together with a decrease in the deoxy-Hb concentration (Fig. 2, left side panels). The oxy-Hb concentration decreased during the succeeding 15 sec of the NWM exploration period and further decreased in the subsequent WM presentation period. This tendency was most obvious

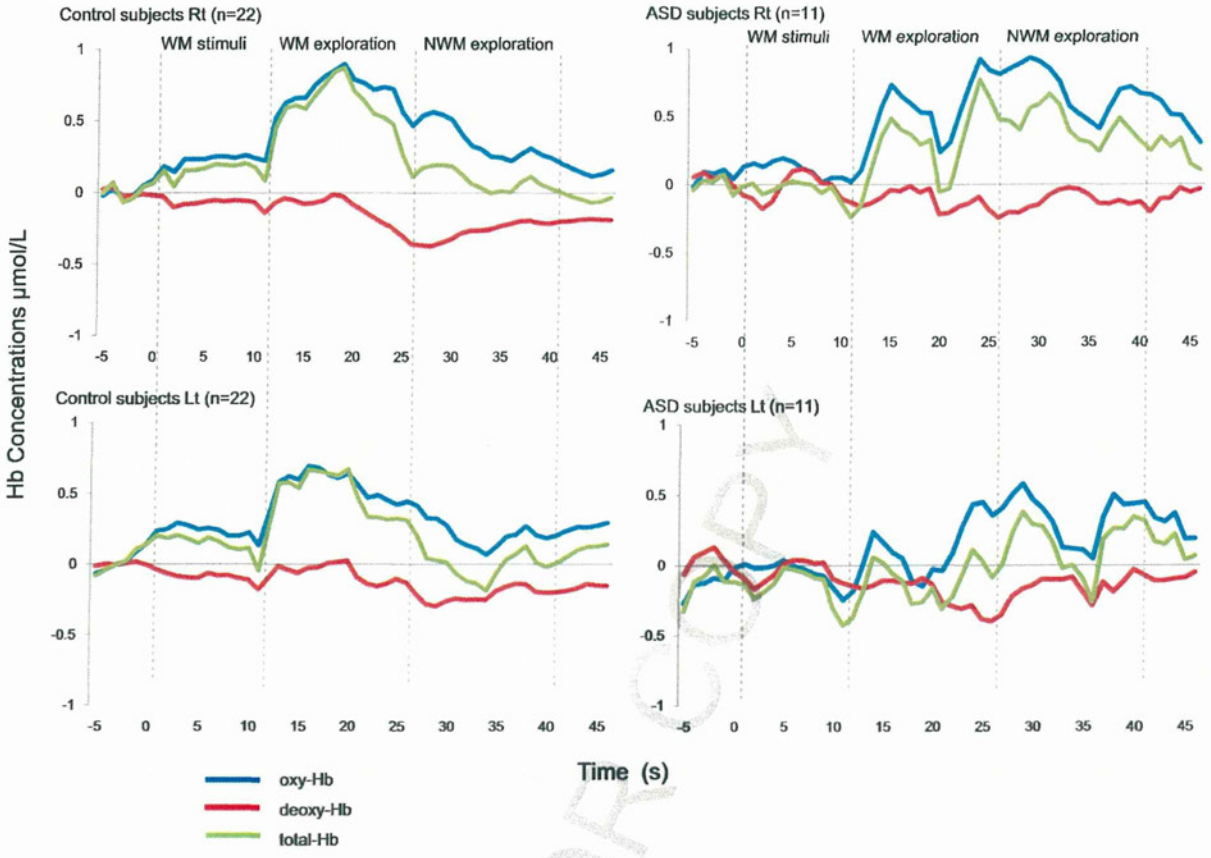

Fig. 3. The near-infrared spectroscopy data of task block No.3 was extracted and averaged for the groups. The left panels (upper panel: right prefrontal cortex, lower panel: left prefrontal cortex) represent the average oxy-hemoglobin (Hb) (blue lines), deoxy-Hb (red lines), and total Hb (green lines) concentration changes as a function of task switch in the controls. The right panels show the same results for the autism spectrum disorder subjects.

in task blocks 3, 4 and 5, and was observed in the right and left PFC. In contrast, changes in the oxy-Hb concentration according to task processing were not obvious in ASD subjects (Fig. 2, right side panels).

To further assess this difference between controls and ASD subjects, the data were reanalyzed with baseline correction by extracting only task block 3 for each subject and the average values in each group were then plotted as shown in Fig. 3. Clear discrimination of PFC activation pattern according to the task switch (i.e., WM stimuli-WM exploration-NWM exploration) observed in controls was absent in ASD subjects.

To assess the effect of task switching on hemodynamics, we calculated the mean oxy-Hb concentration of the 15-sec exploration period for each task (WM and NWM). Figure 4 shows the task wise changes in the mean oxy-Hb concentration in both the right and left sides of PFC (task blocks 1–6 of the WM-NWM task sets) of controls (Fig. 4, left side panel) and ASD subjects (Fig. 4, right side panel). In controls, the mean oxy-Hb concentration increased during WM, decreased during NWM, and gradually increased with an increase in task block number, suggesting that in the control PFC, hemodynamic activity significantly changed as memory load increased according to the task switch. In addition, right PFC laterality was, consistently observed in controls, which is predictable from the nature of the task paradigm that required spatial cognition. In contrast, ASD subjects did not show clear changes in PFC oxygenation according to the WM-NWM switch and obvious right PFC laterality was not observed.

Statistical analysis using the Mann-Whitney-Wilcoxon test was performed to compare the task-switching effect between corresponding WM-NWM task sets in the same task block. As shown, in Fig. 4, among the control subjects, the WM-NWM compar-

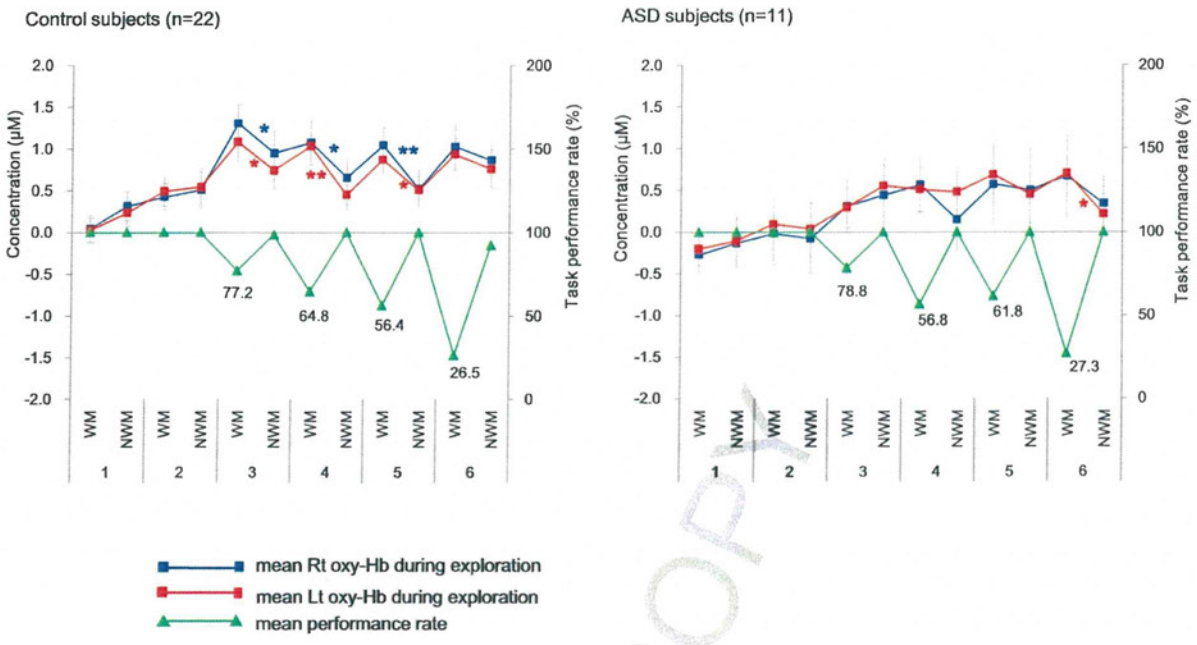

Fig. 4. The mean oxy-hemoglobin (blue lines: right prefrontal cortex, red lines: left prefrontal cortex) concentrations during the exploration period of each task and the task performance rates (green lines) are shown. Left panel: controls, Right panel: Autism spectrum disorder subjects. The left longitudinal axis indicates the relative oxy-hemoglobin concentration (μM), and the right axis indicates the task performance rate (%). The error bar indicates the standard error of the mean.

ison for task blocks 3 (Rt: $P = 0.017$, $Z = -2.386$; Lt: $P = 0.017$, $Z = -2.386$), 4 (Rt: $P = 0.014$, $Z = -2.451$; Lt: $P = 0.004$, $Z = -2.906$) and 5 (Rt: $P = 0.003$, $Z = -3.003$; Lt: $P = 0.039$, $Z = -2.062$) showed a significant difference in the oxy-Hb concentration for both the right and left PFCs. In ASD subjects, a significant difference was only detected in task block 6 for left PFC ($P = 0.021$, $Z = -2.312$).

The mean task performance rate was calculated among the groups. Both controls and ASD subjects showed a gradual decrease in the task performance rate with increasing task block number during the WM task in contrast to that during the NWM task, which was almost 100% for each task block (Fig. 4). ASD subjects showed an insignificant slightly higher mean task performance rate in task blocks 3, 5 and 6 compared to controls.

4. Discussion

In this study using NIRS, we demonstrated the tendency of an evoked CBO increase and decrease in response to task switching in the control subjects but not in ASD subjects. The switching paradigm used alternating WM and NWM tasks and the WM tasks progressively increased memory load. A significant difference in the mean oxy-Hb concentration was observed between WM and NWM exploration periods in task blocks 3, 4 and 5, which suggest that these WM tasks particularly induced a rapid regional CBO increase in the prefrontal measurement areas, which was quickly terminated with subsequent NWM task initiation.

This tendency was not obvious in ASD subjects in the early task blocks of the WM-NWM tasks. However, a weak WM task-dependent oxy-Hb increase was observed from task block 5 and above, but a statistical difference between WM and NWM tasks was found only in task block 6 for the left PFC.

Despite this obvious discrepancy in PFC hemodynamics, the mean task performance rate was similar between controls and ASD subjects. In both groups, the average correct answer rate for the WM tasks gradually decreased as memory load increased, while the NWM performance rate remained almost 100% through all tasks.

These results are consistent with those from a study conducted by Ozonoff and Strayer [15], who used geometric shapes, colored boxes, and three different

WM tasks. However, their study failed to report any significant difference in performance between the autistic, Tourette syndrome, and control groups. The nature of the tasks with colored shapes and the results that showed no significant difference between ASD subjects and controls were similar to those in our study, indicating that depending on the methodology, nature of the task, and characteristics of the participants, WM task performance itself is not always impaired in ASD patients. Nevertheless, continuous functional analysis of hemodynamics during task performance in our study showed a significant difference between controls and ASD subjects, especially in the pattern of response when the task nature changed.

One possible reason for this is ectopic activation of the brain in ASD subjects. Koshino et al. [32] suggested that autistic individuals more often tend to utilize the posterior regions of the brain to solve a WM n-back task with alphabetical letters as stimuli, i.e., they rely on lower visual signal processing rather than the left temporal region of the brain. This result suggested that spatial WM task performance in ASD subjects may be observed by ectopic neural systems or that functional connectivity differs from that activated in normal subjects.

In our present study, a significant difference between WM and NWM exploration components was observed in task blocks 3, 4 and 5 for controls, which may indicate a significant change in brain usage in response to switching of the task. In fact, this is visible in NIRS as a swift hemodynamic change when task switching occurs. Of the tasks used in this study, WM stimuli and NWM exploration components are believed to require more visual processing than the WM exploration component, which mainly requires DLPFC activation [8–10]. This explains the significant change in the PFC oxy-Hb concentration on task switching in controls. Based on the observations of previous studies and the present study, our data could be interpreted as further evidence of a difference in brain signal processing between ASD subjects and controls for tasks involving executive brain functions including spatial WM, especially when memory loads are moderate.

It is interesting that ASD subjects showed no tendency toward task-dependent changes in the PFC oxy-Hb concentration during the early task blocks, but later showed a weak switching tendency (i.e., task blocks 5 and 6; significant difference only in 6, left side). Considering that higher executive functions such as planning, flexible strategy, and organized searching would be more frequently required for later WM task blocks, the PFC oxy-Hb concentration in ASD subjects during later task blocks may indicate a shift in functional connectivity usage from the posterior domain to the prefrontal domain. This shift may be caused by an overload in lower visual processing.

Another possible explanation of the difference between controls and ASD subjects is the lack of DMN regulation in ASD subjects. Daniels et al. [33] showed functional connectivity in patients with posttraumatic stress disorder during WM processing. In their study, greater connectivity was evident between the medial PFC during the verbal WM task, where it is normally suppressed during WM processing. Inadequate DMN activation (i.e., lack of deactivation due to stimuli) in ASD subjects during cognitive tasks such as the Stroop task has also been reported by Kennedy and Courchesne [21] using functional connectivity MRI. Thus, the results observed in ASD subjects may indicate an irregular activation of default mode functional connectivity in PFC.

Combining these observations and those of previous studies, it is reasonable that neurofunctional defects in ASD subjects may not only be due to hypoactivation of task responsible brain regions but also due to a complex disorder that includes DMN defects. Considering that a certain amount of PFC activation is required in response to task switching itself [34], lack of deactivation of resting functional connectivity may lead to a delay in switching and a slow response to incoming tasks in PFC. This may activate ectopic functional connectivity that includes lower WM signal processing and posterior brain activity, although this conclusion cannot be reached definitively from our two-channel NIRS data.

When evaluating the data, it should be kept in mind that NIRS measures changes in blood oxygenation, including intracranial and extracranial tissues [35], and that the measured values indicate an average within the illuminated area. Furthermore, continuous waves of NIRS do not yield absolute values for changes in the Hb concentration without information regarding the optical path length in each subject [36]. However, the changes induced by neuronal activation are believed to indicate changes in CBO and hemodynamics within the activated cortices [23,25,31]. Moreover, the optical path length was relatively homogeneous in the forehead as compared to other re-

gions of the brain, such as the frontal-temporal junction [37]. Therefore, data analysis undertaken in the present study, which only focused on relative intra-task comparison within the continuous performance of the task-switching paradigm, is valuable.

Although the number of functional neurophysiological studies using NIRS is increasing, investigations using NIRS in ASD or other relevant neuropsychological disorders are still limited. We have found only a few studies on schizophrenia patients that describe impairment in prefrontal hemodynamics during multiple tasks including visuospatial WM [38] and the Tower of Hanoi, a classic WM task [39]. These studies suggested a difference between the affected subjects and controls. However, since neither study measured continuous hemodynamic changes during the entire task session, it is difficult to discuss the relevance of ectopic activation or DMN deactivation deficiency during the task. We previously reported continuous measurement by NIRS during two different tasks [27], which enabled us to understand that drastic changes in hemodynamics could occur depending on the nature of the task.

Since one of the characteristic clinical features of ASD is the lack of normal and natural shifts in response to external stimuli [40,41], the delayed or altered switching of functional connectivity in response to incoming stimuli observed in the present study could lead to new insights into the higher executive dysfunctions of ASD. NIRS is a convenient and non-invasive tool with fewer restrictions than fMRI; it allows subjects to perform a number of task sets continuously during measurement, and it has a wide potential application in ASD research for investigating the issues underlying PFC functional connectivity related to switching stimuli. Although the present study was conducted with a limited number of subjects, it is the first to report hemodynamic changes in ASD subjects with continuous observation of PFC during the repetition of tasks of a different nature.

Further investigations should be performed in order to elucidate functional alterations in network connectivity during WM performance in ASD subjects.

Acknowledgement

We are grateful to Dr. Masahiro Tanida for technical advice regarding the present study. This work was, supported by Grants-in-Aid for Scientific Research of the Japan Society for the Promotion of Science, the Academic Research Promotion Fund in Japan, and a research grant from the Ministry of Health, Labor, and Welfare of Japan.

References

[1] Charman T, Baird G. Practitioner review: Diagnosis of autism spectrum disorder in 2- and 3-year-old children. J Child Psychol Psychiatry 2002; 43(3): 289-305.
[2] Filipek PA, Accardo PJ, Baranek GT, Cook EH Jr, Dawson G, Gordon B, et al. The screening and diagnosis of autistic spectrum disorders. J Autism Dev Disord 1999; 29(6): 439-84. Erratum in: J Autism Dev Disord 2000; 30(1): 81.
[3] Hill EL. Executive dysfunction in autism. Trends Cogn Sci 2004; 8(1): 26-32.
[4] Castelli F, Frith C, Happé F, Frith U. Autism, Asperger syndrome and brain mechanisms for the attribution of mental states to animated shapes. Brain 2002; 125(Pt 8): 1839-49.
[5] Deuel RK. Autism: a cognitive developmental riddle. Pediatr Neurol 2002; 26(5): 349-57.
[6] Happé F, Ronald A, Plomin R. Time to give up on a single explanation for autism. Nat Neurosci 2006; 9(10): 1218-20.
[7] Baddeley AD. Working memory. Oxford: Oxford University Press; 1986.
[8] Braver TS, Cohen JD, Nystrom LE, Jonides J, Smith EE, Noll DC. A parametric study of prefrontal cortex involvement in human working memory. Neuroimage 1997; 5(1): 49-62.
[9] Cabeza R, Dolcos F, Graham R, Nyberg L. Similarities and differences in the neural correlates of episodic memory retrieval and working memory. Neuroimage 2002; 16(2): 317-30.
[10] Carlson S, Martinkauppi S, Rämä P, Salli E, Korvenoja A, Aronen HJ. Distribution of cortical activation during visuospatial n-back tasks as revealed by functional magnetic resonance imaging. Cereb Cortex 1998; 8(8): 743-52.
[11] Hughes C, Russell J, Robbins TW. Evidence for executive dysfunction in autism. Neuropsychologia 1994; 32(4): 477-92.
[12] Minshew NJ, Luna B, Sweeney JA. Oculomotor evidence for neocortical systems but not cerebellar dysfunction in autism. Neurology 1999; 52(5): 917-22.
[13] Steele SD, Minshew NJ, Luna B, Sweeney JA. Spatial working memory deficits in autism. J Autism Dev Disord 2007; 37(4): 605-12.
[14] Griffith EM, Pennington BF, Wehner EA, Rogers SJ. Executive functions in young children with autism. Child Dev 1999; 70(4): 817-32.
[15] Ozonoff S, Strayer DL. Further evidence of intact working memory in autism. J Autism Dev Disord 2001; 31(3): 257-63.
[16] Russell J, Jarrold C, Henry L. Working memory in children with autism and with moderate learning difficulties. J Child Psychol Psychiatry 1996; 37(6): 673-86.
[17] Luna B, Minshew NJ, Garver KE, Lazar NA, Thulborn KR, Eddy WF, et al. Neocortical system abnormalities in autism: an fMRI study of spatial working memory. Neurology 2002; 59(6): 834-40.
[18] Ring HA, Baron-Cohen S, Wheelwright S, Williams SC, Brammer M, Andrew C, et al. Cerebral correlates of preserved cognitive skills in autism: a functional MRI study of embedded figures task performance. Brain 1999; 122(Pt 7): 1305-15.

[19] Rogers BP, Morgan VL, Newton AT, Gore JC. Assessing functional connectivity in the human brain by fMRI. Magn Reson Imaging 2007; 25(10): 1347-57.
[20] Buckner RL, Andrews-Hanna JR, Schacter DL. The brain's default network: anatomy, function, and relevance to disease. Ann N Y Acad Sci 2008; 1124: 1-38.
[21] Kennedy DP, Redcay E, Courchesne E. Failing to deactivate: resting functional abnormalities in autism. Proc Natl Acad Sci U S A 2006; 103(21): 8275-80.
[22] Kennedy DP, Courchesne E. The intrinsic functional organization of the brain is altered in autism. Neuroimage 2008; 39(4): 1877-85.
[23] Sakatani K, Xie Y, Lichty W, Li S, Zuo H. Language-activated cerebral blood oxygenation and hemodynamic changes of the left prefrontal cortex in poststroke aphasic patients: a near-infrared spectroscopy study. Stroke 1998; 29(7): 1299-304.
[24] Sakatani K, Chen S, Lichty W, Zuo H, Wang YP. Cerebral blood oxygenation changes induced by auditory stimulation in newborn infants measured by near infrared spectroscopy. Early Hum Dev 1999; 55(3): 229-36.
[25] Sakatani K, Lichty W, Xie Y, Li S, Zuo H. Effects of aging on language-activated cerebral blood oxygenation changes of the left prefrontal cortex: Near infrared spectroscopy study. J Stroke Cerebrovasc Dis 1999; 8(6): 398-403.
[26] Sakatani K, Yamashita D, Yamanaka T, Oda M, Yamashita Y, Hoshino T, et al. Changes of cerebral blood oxygenation and optical pathlength during activation and deactivation in the prefrontal cortex measured by time-resolved near infrared spectroscopy. Life Sci 2006; 78(23): 2734-41.
[27] Murata Y, Sakatani K, Hoshino T, Fujiwara N, Kano T, Nakamura S, et al. Effects of cerebral ischemia on evoked cerebral blood oxygenation responses and BOLD contrast functional MRI in stroke patients. Stroke 2006; 37(10): 2514-20.
[28] Tanida M, Sakatani K, Takano R, Tagai K. Relation between asymmetry of prefrontal cortex activities and the autonomic nervous system during a mental arithmetic task: near infrared spectroscopy study. Neurosci Lett 2004; 369(1): 69-74.
[29] Tanida M, Katsuyama M, Sakatani K. Relation between mental stress-induced prefrontal cortex activity and skin conditions: a near-infrared spectroscopy study. Brain Res 2007; 1184: 210-6.
[30] Homan RW, Herman J, Purdy P. Cerebral location of international 10-20 system electrode placement. Electroencephalogr Clin Neurophysiol 1987; 66(4): 376-82.
[31] Hock C, Villringer K, Müller-Spahn F, Wenzel R, Heekeren H, Schuh-Hofer S, et al. Decrease in parietal cerebral hemoglobin oxygenation during performance of a verbal fluency task in patients with Alzheimer's disease monitored by means of near-infrared spectroscopy (NIRS)--correlation with simultaneous rCBF-PET measurements. Brain Res 1997; 755(2): 293-303.
[32] Koshino H, Carpenter PA, Minshew NJ, Cherkassky VL, Keller TA, Just MA. Functional connectivity in an fMRI working memory task in high-functioning autism. Neuroimage 2005; 24(3): 810-21.
[33] Daniels JK, McFarlane AC, Bluhm RL, Moores KA, Clark CR, Shaw ME, et al. Switching between executive and default mode networks in posttraumatic stress disorder: alterations in functional connectivity. J Psychiatry Neurosci 2010; 35(4): 258-66.
[34] Dove A, Pollmann S, Schubert T, Wiggins CJ, von Cramon DY. Prefrontal cortex activation in task switching: an event-related fMRI study. Brain Res Cogn Brain Res 2000; 9(1): 103-9.
[35] van der Zee P, Cope M, Arridge SR, Essenpreis M, Potter LA, Edwards AD, et al. Experimentally measured optical pathlengths for the adult head, calf and forearm and the head of the newborn infant as a function of inter optode spacing. Adv Exp Med Biol 1992; 316: 143-53.
[36] Delpy DT, Cope M, van der Zee P, Arridge S, Wray S, Wyatt J. Estimation of optical pathlength through tissue from direct time of flight measurement. Phys Med Biol 1988; 33(12): 1433-42.
[37] Zhao H, Tanikawa Y, Gao F, Onodera Y, Sassaroli A, Tanaka K, et al. Maps of optical differential pathlength factor of human adult forehead, somatosensory motor and occipital regions at multi-wavelengths in NIR. Phys Med Biol 2002; 47(12): 2075-93.
[38] Quaresima V, Giosuè P, Roncone R, Casacchia M, Ferrari M. Prefrontal cortex dysfunction during cognitive tests evidenced by functional near-infrared spectroscopy. Psychiatry Res 2009; 171(3): 252-7.
[39] Ikezawa K, Iwase M, Ishii R, Azechi M, Canuet L, Ohi K, et al. Impaired regional hemodynamic response in schizophrenia during multiple prefrontal activation tasks: a two-channel near-infrared spectroscopy study. Schizophr Res 2009; 108(1-3): 93-103.
[40] Courchesne E, Townsend J, Akshoomoff NA, Saitoh O, Yeung-Courchesne R, Lincoln AJ, et al. Impairment in shifting attention in autistic and cerebellar patients. Behav Neurosci 1994; 108(5): 848-65.
[41] Robinson S, Goddard L, Dritschel B, Wisley M, Howlin P. Executive functions in children with autism spectrum disorders. Brain Cogn 2009; 71(3): 362-8.

Int. J. Devl Neuroscience 31 (2013) 138–144

Contents lists available at SciVerse ScienceDirect

International Journal of Developmental Neuroscience

journal homepage: www.elsevier.com/locate/ijdevneu

Morphology of the facial motor nuclei in a rat model of autism during early development

Akiko Oyabu, Yasura Tashiro*, Takahiro Oyama, Kensaku Ujihara, Takeshi Ohkawara, Michiru Ida-Eto, Masaaki Narita

Department of Anatomy II, Graduate School of Medicine, Mie University, Japan

ARTICLE INFO

Article history:
Received 9 October 2012
Received in revised form
22 November 2012
Accepted 8 December 2012

Keywords:
Cranial motor nuclei
Migration
Autism
Hindbrain
Rat embryo

ABSTRACT

The development of facial nuclei in animal models of disease is poorly understood, but autism is sometimes associated with facial palsy. In the present study, to investigate migration of facial neurons and initial facial nucleus formation in an animal model of autism, rat embryos were treated with valproic acid (VPA) *in utero* at embryonic day (E) 9.5 and their facial nuclei were analyzed by *in situ* hybridization at E13.5, E14.5 and E15.5. Signals for *Tbx20*, which is expressed in early motor neurons, appeared near the floor plate at the level of the vestibular ganglion and extended caudolaterally, where they became ovoid in shape. This pattern of development was similar between control and VPA-exposed embryos. However, measurements of the migratory pathway and the size of the facial nuclei revealed that exposure to VPA hindered the caudal migration of neurons to the facial nuclei. Signals for *cadherin 8*, which is expressed in mature facial nuclei, revealed that exposure to VPA caused a significant reduction in the size of the facial nuclei. Our findings provide the first quantitative description of tangential migration and nucleus formation in the developing hindbrain in a rat model of autism.

1. Introduction

Neural migration is one of the pivotal first steps in precisely establishing the neural network, and both radial and tangential migrations contribute to the organization of the cortex into layers and nucleus formation in the developing brain. Numerous recent studies comparing the time courses of neural migration in wild-type and transgenic animals have revealed that a combination of molecules regulates the direction of neural migration (**Bloch-Gallego et al., 2005; Chédotal and Rijli, 2009; Chédotal, 2010; Hatten, 1999; Huang, 2009**).

Developing facial nuclei migrate tangentially within the hindbrain. During early development, neurons that will eventually form the facial nuclei are generated in rhombomere 4 (r4) then migrate caudally to r6 to the site of the facial nuclei (**Chandrasekhar, 2004; Hatten, 1999; Noden, 1993; Yamamoto and Schwarting, 1991**). Studies using transgenic mice, both *in vivo* and *in vitro* with cells derived from these mice, have identified some of the molecules that are responsible for regulating tangential migration (**Chédotal and Rijli, 2009; Huang, 2009**). However, the development and migration of neurons to the facial nuclei are poorly understood in animal models of disease.

Autism spectrum disorders (ASDs) are neurodevelopmental disorders characterized by impairments in social interaction and communication, and are associated with repetitive behaviors and interests (**Charman and Baird, 2002; Filipek et al., 1999**). An association of autism with facial nerve (7th cranial nerve) palsy has been described in several cases of thalidomide embryopathy, Möbius sequence, CHARGE association and Goldenhar syndrome (**Gillberg and Winnergård, 1984; Miller et al., 2005; Ornitz et al., 1977**). Given this association, a more precise understanding of the development of the facial nuclei, from which facial nerves originate, in ASD patients, could potentially be indispensable for elucidating the pathogenesis of autism with facial palsy.

Rodent models of autism have been particularly useful for elucidating the association of autism with embryonic development of the nervous system. Epidemiological studies had revealed that exposure to thalidomide (THAL) or valproic acid (VPA) during the first trimester of pregnancy causes a higher incidence of autism in human offspring (**Strömland et al., 1994; Williams et al., 2001**); based on this, a rat model of autism was generated by prenatal THAL or VPA exposure (**Narita et al., 2002**). In studies using this model, behavioral, biochemical and neuroanatomic similarities between human cases of autism and rats exposed to VPA *in utero* were observed (**Ingram et al., 2000; Miyazaki et al., 2005; Narita Naoko et al., 2002; Narita Masaaki et al., 2010; Rodier et al., 1996, 1997**).

* Corresponding author at: Department of Anatomy II, Graduate School of Medicine, Mie University, 2-174 Edobashi, Tsu, Mie 514-8507, Japan. Tel.: +81 59 231 9938; fax: +81 59 231 9938.
E-mail address: ytashiro@doc.medic.mie-u.ac.jp (Y. Tashiro).

0736-5748/$36.00 © 2012 ISDN. Published by Elsevier Ltd. All rights reserved.
http://dx.doi.org/10.1016/j.ijdevneu.2012.12.002

Thus, our rat models of autism are well suited for investigations of the embryonic development of the nervous system.

Although the embryonic development of facial nerves in our rat model of autism has not been fully characterized, embryonic VPA treatment has been shown to reduce the number of adult motor neurons, including those of the facial nuclei (Rodier et al., 1996), resulting in anatomical anomalies within the cranial motor nuclei. Moreover, we previously reported on morphological abnormalities in the peripheral facial nerves in an embryonic rat model of autism (Tashiro et al., 2011). In these rats, peripheral facial nerves became truncated and defasciculated (Tashiro et al., 2011). In addition, Ornoy (2009) reviewed the relationship between VPA and autism, including experiments using VPA to generate animal models of autism, and concluded that experimental animal models generally mimic the effects of VPA in man, although animals seem to be more resistant to VPA than humans. Taken together, these findings suggest that the development of facial neurons, not only in the peripheral nerves but also in the central hindbrain, including the facial nuclei, should be examined after VPA exposure.

In the present study, to examine the caudal migration of neurons and the initial formation of facial nuclei in a rat model of autism, VPA was administered to pregnant rats at E9.5. This enables delivery to the embryos *via* the placenta and subsequent distribution to the facial nuclei. We utilized a combination of flat whole-mount preparations and *in situ* hybridization for molecular markers expressed in the cranial motor neurons to allow us to clearly identify the facial nuclei and quantify their size for statistical analysis.

2. Material and methods

2.1. Animals and teratogen exposure

All experiments involving animals were approved by the Community of Laboratory Animal Research Center at the University of Mie, Japan. Details of the teratogen administration have been previously described (Miyazaki et al., 2005; Narita Naoko et al., 2002; Narita Masaaki et al., 2010). In brief, female Wistar rats (2–6 months old) were mated overnight and the day of insemination was designated as embryonic day (E) 0.5. On E9.5, at 1:00 p.m., 800 mg/kg VPA was administered orally without sedation to dams in each group using an infant feeding tube (Atom Medical, Tokyo, Japan) attached to a 2.5 ml disposable syringe. We referred to prior animal experiments using these teratogens to determine the doses of VPA (Ingram et al., 2000). Because our previous study showed that VPA exposure after E9.5 induced morphological abnormalities of facial nerves (Tashiro et al., 2011), we adopted E9.5 as the day of administration. VPA was prepared by dissolving the drug in 5% arabic gum in distilled water. No pregnant mothers died from the dose of VPA, and most embryos survived.

2.2. Flat whole-mount preparations of rat hindbrain

Embryos were removed from the dams at E13.5, E14.5 or E15.5, and the crown–rump length (CRL) was measured at each stage. The portion of the head containing the midbrain and hindbrain was dissected out in cold phosphate-buffered saline (PBS). To obtain flat whole-mount preparations of the hindbrain, the dorsal midline of the neural tube was completely cut and the 4th ventricle was opened. The isthmus of the midbrain–hindbrain boundary was cut, and the hindbrain was carefully freed from the meninges and surrounding tissue while keeping the trigeminal ganglion and vestibular ganglion, as well as their roots, intact.

Flat whole-mounted hindbrains were fixed in 4% paraformaldehyde in PBS for 7–10 h at 4 °C. Tissues were then washed twice with Tris-buffered saline (TBS), dehydrated through a graded methanol/TBS series at 4 °C, and stored in 100% methanol at −20 °C.

In observing tissues under a microscope, to ensure equal pressure across whole-mounted hindbrains, multiple layers of plastic tape were inserted as supports between the slide and coverslip. Because the layered plastic tape supports the load from the coverslip, the preparations received equal pressure in all locations and were not transformed by unequal pressure.

2.3. In situ hybridization

A DNA fragment corresponding to a portion of rat *Tbx20* (nucleotides 51–885, GenBank NM_001108132) or *cdh8* (nucleotides 1909–2435, GenBank NM_053393.2) cDNA was cloned into the pGEM-T Easy vector (Promega, La Jolla, CA). Using this plasmid as a template, sense and antisense single-strand RNA probes were synthesized using a digoxigenin labeling kit (Roche Diagnostics, Tokyo, Japan). Whole-mount *in situ* hybridization using sense probes detected no signal except background noise, demonstrating specific hybridization to the target sequences.

In situ hybridization on flat whole-mounted hindbrains was performed according to the methods of Nieto et al. (1996), with minor modifications. Tissues were treated with 0.3% H_2O_2/methanol for 30 min and rehydrated through a graded methanol/PBST series. The hindbrains were then treated with 10 μg/ml proteinase K/PBST and fixed in 0.2% glutaraldehyde/4% paraformaldehyde in PBS. After rinsing three times for 5 min in PBST, they were prehybridized in prehybridization solution (50% formamide; 5 × SSC; 50 μg/ml yeast RNA (Roche); 50 μg/ml heparin (Roche); 5 mM EDTA; 1% SDS). Tissue was then incubated in hybridization solution (prehybridization solution containing 1 mg/ml probe) overnight at 60 °C. After high-stringency washes, the tissues were blocked for 2 h in blocking reagent (Roche) and incubated in a 1/500 dilution of anti-digoxigenin-AP conjugate (Roche) in blocking reagent for 3 h. After an overnight wash with TBST, the signals were visualized in NTMT (0.1 M Tris–HCl, 0.1 M NaCl, 0.05 M $MgCl_2$, and 0.1% Tween 20) containing nitroblue tetrazolium chloride/5-bromo-4-chloro-3-indolyl phosphate, toluidine salt (Roche).

2.4. Statistical analysis

Embryos from at least three different dams were analyzed for each condition. Bilateral facial nuclei were analyzed in each embryo and the number of analyzed facial nuclei pairs is referred to in the text as "*n*=". Digital images were captured using a light microscope equipped with a CCD camera (DXM1200F, Nikon, Tokyo, Japan). The intensities of *Tbx20* or *cdh8* signals and the sizes of the areas circumscribed by these signals were measured using Image J software. Signal intensity was defined such that complete white was scored as "0" and complete black as "255". The relative level of signal intensity was determined by comparison with the signal intensity in the control group. The boundaries of these regions were determined based on the signal threshold, excluding background noise. The mean and standard deviation (SD) was calculated, and differences among developmental stages were evaluated using *t*-tests.

3. Results

3.1. Development of Tbx20-positive facial motor neurons

To elucidate the development of the cranial motor nuclei within the hindbrain, in relation to the rostrocaudal and dorsoventral axes, flat whole-mount preparations (Fig. 1) from E13.5, 14.5 and 15.5 embryos were analyzed. Flat whole-mount embryonic hindbrain preparations were subjected to *in situ* hybridization using an RNA probe for *Tbx20*, which is expressed in early cranial motor neurons (Figs. 2 and 3).

In whole-mount preparations from control embryos at E13.5, intense *Tbx20* signals were observed near the floor plate between the vestibular ganglia, corresponding to r4 at the rostrocaudal level (Fig. 2A). Weak *Tbx20* signals were observed in the ventral column lateral to the floor plate (data not shown). In whole-mount preparations from embryos exposed to VPA *in utero*, the pattern of *Tbx20* expression was similar (Fig. 2B).

At E14.5 in the control group, *Tbx20* signals extended from r4 through r5–6 in a caudolateral direction (Fig. 2C, arrows). Toward the caudal end of the *Tbx20* expression domain, the signal faded out (Fig. 2C, arrowheads). These signal patterns were similar to those observed in the VPA-exposed group (Fig. 2D).

Because flat whole-mount preparations are much thicker at E15.5 than they are at earlier stages, *Tbx20* signals could be observed more clearly from either the ventricular or pial sides (Fig. 3). In the control group, despite limited *Tbx20* expression near the floor plate on the ventricular side (Fig. 3A, arrows), the caudal end of the *Tbx20* signals was located on the pial side and had an ovoid appearance (Fig. 3C, asterisks). In addition, intense *Tbx20* signals were also observed between the trigeminal ganglia, corresponding to r2 at the rostrocaudal level on the pial side (Fig. 3C and D, arrowheads).

In the VPA-exposed group, the pattern of *Tbx20* expression was similar (Fig. 3B and D). However, the signals near the floor plate were more intense than those in the control

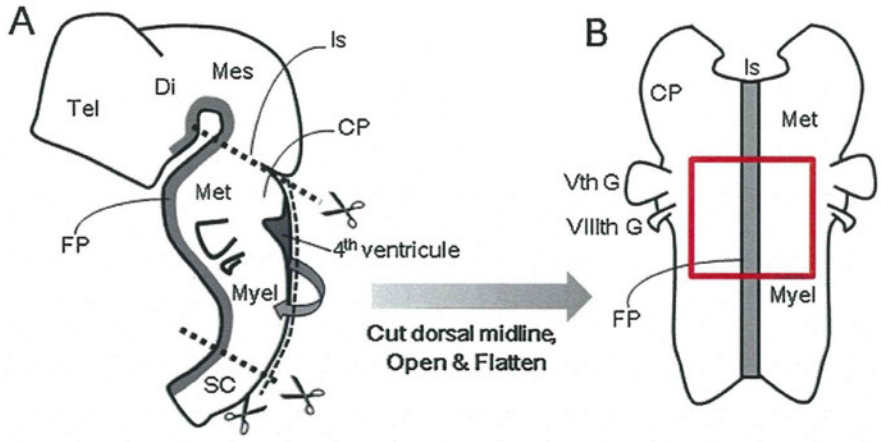

Fig. 1. Flat whole-mount preparation of the hindbrain. (A) Schematic diagram showing the cut site in the neural tube. Embryonic rat hindbrains were dissected and oriented with the ventricular side down (Tashiro et al., 2000). (B) Schematic diagram of a flat whole-mount preparation of the hindbrain. Figs. 2, 3 and 5 correspond to the area outlined by the red square in B. CP: cerebellar plate, Di: diencephalon, FP: floor plate, Is: isthmus, Mes: mesencephalon, Met: metencephalon, Myel: myelencephalon, Tel: telencephalon, SC: spinal cord, Vth G: trigeminal ganglion, VIIIth G: vestibular ganglion. (For interpretation of the references to color in this figure legend, the reader is referred to the web version of the article).

group (Fig. 3B, arrows) and the oval *Tbx20*-positive region appeared to be smaller than it was in controls (Fig. 3C and D, asterisks). The pattern of *Tbx20* signals near the floor plate was considered to represent the migratory pathway of facial motor neurons, and the oval areas positive for *Tbx20* signals at the caudal end were considered to represent the facial nuclei.

To identify differences in the migratory pathways and the sizes of facial nuclei between control and VPA-exposed groups, the *Tbx20*-positive areas were measured. The area of the *Tbx20*-positive migratory pathway ($\times 10^4\ \mu m^2$) was 0.66 ± 0.17 in the control group ($n = 6$) and 1.37 ± 0.31 in the VPA-exposed group ($n = 12$), revealing a significant increase in the size of the pathway in embryos exposed to VPA compared with controls ($p < 0.001$). The area of the *Tbx20*-positive facial nuclei ($\times 10^4\ \mu m^2$) was 9.33 ± 0.92 in the control group ($n = 6$) and 7.55 ± 1.02 in the VPA-exposed group ($n = 12$), revealing a significant reduction in the size of these nuclei compared with controls ($p < 0.01$). When the sizes of *Tbx20*-positive facial nuclei were plotted against the sizes of *Tbx20*-positive migratory pathways (Fig. 4), the resulting graph showed an inverse relationship between the two, with increasing size of the migratory pathway and

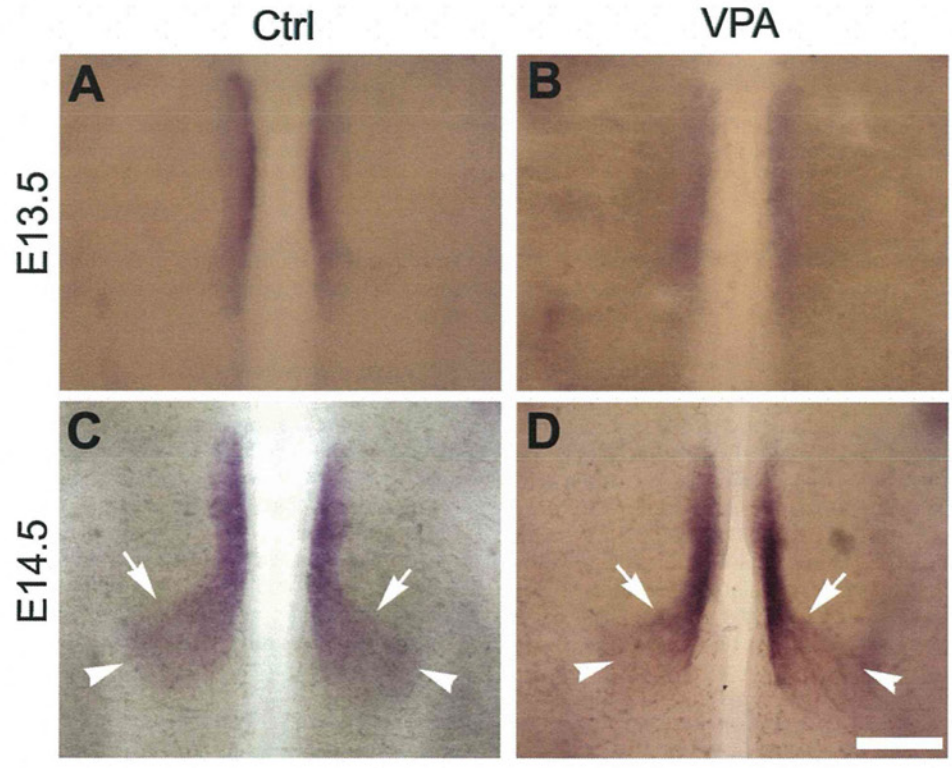

Fig. 2. *Tbx20* expression patterns at E13.5 and E14.5. (A and B) E13.5 preparations showing *Tbx20* signals near the floor plate in the control group (A) and VPA-exposed group (B). (C and D) E14.5 preparations showing *Tbx20* signals near the floor plate in the control group (C) and VPA-exposed group (D). *Tbx20* signals extend in a caudolateral direction (arrows). Near the caudal end of the *Tbx20* expression domain, the signal fades out (arrowheads). Rostral is up. Scale bar: 250 μm.

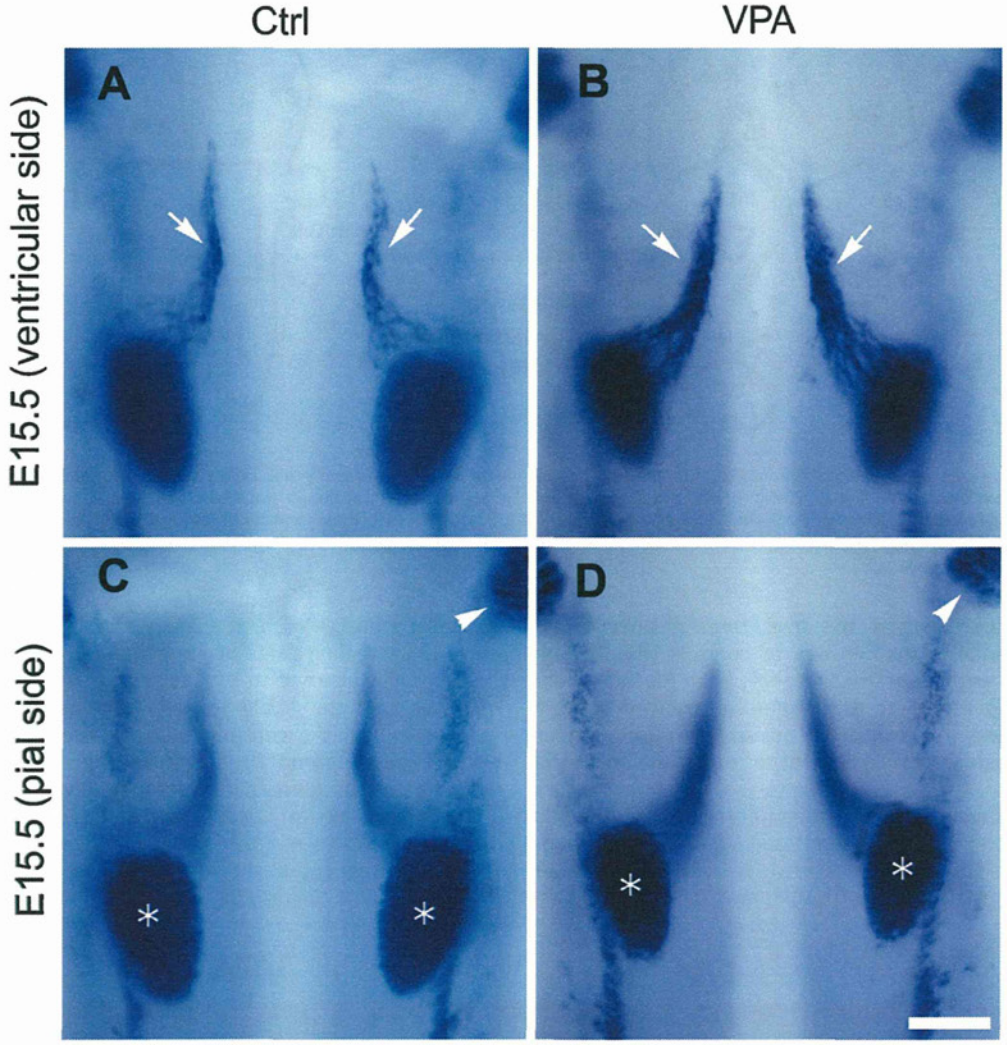

Fig. 3. *Tbx20* expression pattern at E15.5. (A and B) E15.5 preparations, viewed from the ventricular side, showing *Tbx20* signals near the floor plate in the control group (A) and VPA-exposed group (B). Signals in the migratory pathway of the VPA-exposed preparation (B, arrows) are more intense than those in the control preparation (A, arrows). (C and D) E15.5 preparations, viewed from the pial side, showing *Tbx20*-positive facial nuclei in the control group (C) and VPA-exposed group (D). The facial nuclei are smaller in embryos exposed to VPA (D, asterisks) than in control embryos (C, asterisks). Rostral is up. Scale bar: 250 μm.

decreasing size of facial nuclei following VPA exposure ($p < 0.001$; $R = -0.74$).

3.2. Size of facial nuclei

To determine the sizes of mature facial nuclei, the area of *cadherin 8* (*cdh8*) expression was measured (Fig. 5). The *cdh8* gene is expressed in developed facial motor nuclei (Korematsu and Redies, 1997), and is not expressed within the migratory pathway (Fig. 5). The area of the *cdh8*-positive facial nuclei ($\times 10^4\ \mu m^2$) was 9.87 ± 0.43 in the control group ($n = 4$) and 7.06 ± 1.31 in the VPA-exposed group ($n = 5$), revealing a significant reduction in the area of *cdh8* expression in the facial nuclei of VPA-exposed animals ($p < 0.01$). Indeed, the average area of *cdh8*-positive facial nuclei in the VPA-exposed group was 28.4% less than that in the control group.

CRL of E15.5 embryos was also measured. VPA-exposed animals appeared robust and had no external malformations. CRL (mm) was 12.80 ± 0.37 in the control group ($n = 5$) and 12.24 ± 0.18 in the VPA-exposed group ($n = 4$), revealing a significant reduction in CRL in VPA-exposed embryos at E15.5 ($p < 0.05$). The average CRL in VPA-exposed embryos was only 4.3% less than that in control embryos; thus, the reduction in the size of the *cdh8*-positive facial nuclei was not directly proportional to the reduction in average CRL.

3.3. Expression levels of cdh8 in the facial nuclei

To estimate the contribution of the cell adhesion molecule *cadherin 8* to the development of the facial nuclei, a preliminary analysis of the expression levels of *cdh8* was performed. The signal intensity in the VPA-exposed group was normalized to that in the control group, which was designated as 100%. The intensity of the *cdh8* signal in the facial nuclei was 100.0 ± 2.8 in the control group ($n = 4$) and 84.5 ± 12.2 in the VPA-exposed group ($n = 5$), revealing a significant reduction (by 15.5%) in *cdh8* expression in the VPA-exposed group compared with controls ($p < 0.05$).

4. Discussion

We examined the development of facial nuclei in an animal model of autism, established by *in utero* exposure to VPA, using *in situ* hybridization for the molecular markers *Tbx20* and *cdh8*. Analysis of *Tbx20* expression revealed similar patterns of caudal

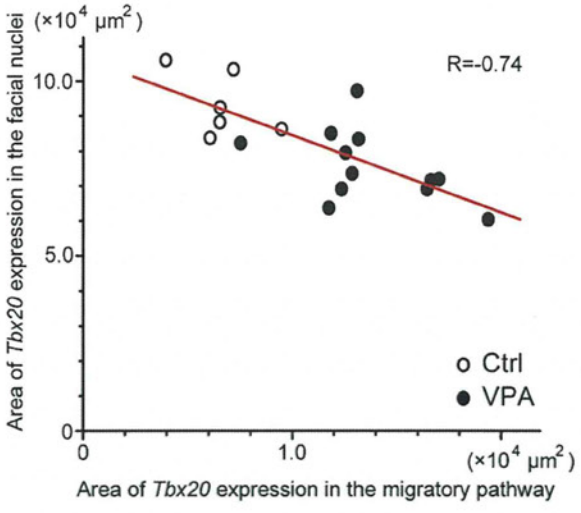

Fig. 4. Correlation between the area of the *Tbx20*-positive migratory pathway and the facial nucleus. The increase in the size of the migratory pathway is inversely proportional to the reduction in the size of the facial nucleus ($p < 0.001$, $R = -0.74$). Open circles: control group, filled circles: VPA-exposed group.

migration of neurons to the facial nuclei in control and VPA-exposed groups; however, this caudal migration of neurons was hindered in animals exposed to VPA, with the result that the facial nuclei were significantly smaller in these animals. Our data provide the first description of tangential migration and nucleus formation in the developing hindbrain in a rat model of autism. Moreover, this disruption during early development of the facial nuclei might contribute to the etiology of autism with facial palsy.

4.1. Technical consideration

To assess the distribution of *Tbx20* and *cdh8* signals in the developing hindbrain, flat whole-mount preparations (**Tashiro et al., 2000, 2007**) were used. These allowed us to observe signal distributions within both the rostrocaudal and dorsoventral axes, without requiring the reconstruction of serial sections. Because later-stage whole-mount preparations are not suitable for an analysis of signal depth, we restricted our observations to the ventricular and pial sides at E15.5.

Facial nuclei were identified based on the expression of *Tbx20* and *cdh8* mRNA signals and their anatomical locations within the flat whole-mount preparations. Because *Tbx20* is expressed in all early-stage cranial motor neurons (**Kraus et al., 2001; Meins et al., 2000; Song et al., 2006**), it was not possible to distinguish the facial nuclei from the abducens or trigeminal motor nuclei. However, using flat whole-mount preparations enabled us to positively identify the migratory pathways taken by neurons to reach these nuclei based on anatomical landmarks as well as the positioning of the ganglia and their roots. The trigeminal ganglion is positioned near rostrocaudal level r2, and *Tbx20* signals near the trigeminal ganglion are considered to represent the trigeminal motor nuclei (**Noden, 1993**). The vestibular ganglion is positioned near rostrocaudal level r4; *Tbx20* signals near the floor plate between these ganglia are considered to represent the facial motor nuclei. The neurons that comprise the facial nuclei originate in r4 and migrate caudally to r6; their migratory pathways are well-described in the literature (**Chandrasekhar, 2004; Hatten, 1999; Noden, 1993; Yamamoto and Schwarting, 1991**) and are consistent with the signal patterns we observed. The expansion of the area of *Tbx20*-positive signals is likely correlated to the migration of neurons to and shape of facial motor nuclei. Thus, the combination of *Tbx20* signals and positional information in flat whole-mount preparations is an appropriate tool for evaluating the development of facial nuclei.

In addition to *Tbx20* signals, *cdh8* signals can be used to visualize mature facial nuclei (**Korematsu and Redies, 1997**). Because *cdh8* is not expressed in the migratory pathways of neurons destined for the facial nuclei or other cranial motor nuclei in the hindbrain, *cdh8* signals enable us to specifically identify the area of the facial nuclei. Quantification of facial nucleus area based on *cdh8* expression is therefore more precise than measurements based on *Tbx20* expression. We have provided the first numerical quantification of the area of the developing facial nuclei following exposure to VPA *in utero*.

4.2. Development of the facial nuclei in a rat model of autism

The caudal migration patterns of neurons destined for the facial nuclei in a rat model of autism induced by VPA exposure were similar to those seen in normal control rats. However, VPA exposure hindered this migration and significantly reduced the area of the facial nuclei. Although CRL was also reduced in the VPA-exposed group, the amount of decrease was less substantial than that for facial nucleus size, indicating that the reduction in the area of the facial nuclei was not due to overall shrinkage of the entire embryo after exposure to VPA. Moreover, the quantified decrease in facial nucleus area suggests an even larger percent decrease in volume: if the shape of the facial nucleus is assumed to be a sphere, then a 28.4% decrease in area equates to about a 40% decrease in volume. Thus, the total size of the facial nuclei is considerably reduced in animals exposed to VPA.

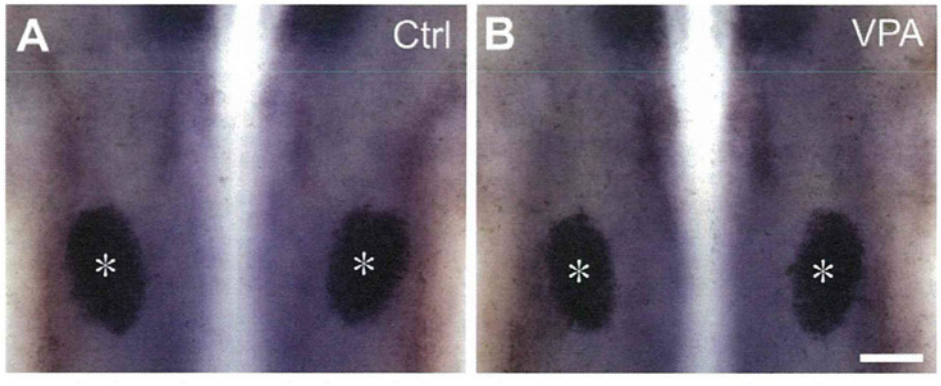

Fig. 5. *Cdh8* expression in the facial nuclei. (A and B) E15.5 preparation, viewed from the pial side, showing *cdh8*-positive facial nuclei in the control group (A) and VPA-exposed group (B). The facial nuclei are smaller in embryos exposed to VPA (B, asterisks) than in control embryos (A, asterisks). Note that *cdh8* signals were not detected in the migratory pathway (see also Fig. 3A and B, arrowheads). Rostral is up. Scale bar: 250 μm.

The reduction in facial nucleus size could be attributed to hindered cell migration, as we observed cells stacked in the migratory pathway, a common characteristic of failed cell migration, in addition to the observed inverse correlation between larger migratory pathway area and smaller facial nucleus size. Accumulating *in vivo* and *in vitro* studies have begun to elucidate the molecular mechanisms underlying the regulation of the caudal migration of neurons to facial motor nuclei in normal fishes and rodents (Bingham et al., 2002; McKay et al., 1997; Song et al., 2006; Studer et al., 1996; Wada et al., 2006). Some cell adhesion molecules, such as cadherin family members (LaMora and Voigt, 2009; Qu et al., 2010), could contribute to this migration by acting as scaffolds or facilitating the interactions between substrates. Therefore, a slight decrease in *cdh8* expression might lead to smaller facial nuclei by disrupting cellular migration. A decrease in *cdh8* expression may also explain the observed defasciculation and misrouting of peripheral facial nerves in the 2nd branchial arch (Tashiro et al., 2011), although the complimentary expression of other adhesion molecules would presumably regulate morphological development in peripheral and central facial nerve regions.

Another possible explanation for the reduction in facial nucleus size is a decreased number of cells within the nuclei given that the birth dates of most of these nuclei correspond to the stage at which VPA treatment was administered. VPA is known to affect cell division and the cell cycle by disturbing histone deacetylation (Chen et al., 2007; Phiel et al., 2001). The neurons of the facial nuclei are produced between days E12 and E14, with peak production at E13 (Altman and Bayer, 1982). In the present study, VPA exposure was performed at E9.5, and the short pharmacokinetic half-life of VPA in rodents (Nau et al., 1981) suggests that the effects of VPA would be limited to a narrow temporal window. Therefore, VPA treatment may reduce the number of early progenitor cells responsible for producing facial neurons. Further analysis of nucleogenesis is needed to clarify this possibility.

The mechanism by which VPA exposure affects the regulation of cell migration or differentiation remains unknown. It is possible that VPA exposure could have changed the identity of the rhombomeres. Various combinations of *Hox* gene expression are used to specify individual rhombomeres as well as to regulate the differentiation of cranial neurons (Erzurumlu et al., 2010; Noden, 1993; Trainor and Krumlauf, 2000; Yamamoto and Schwarting, 1991), and VPA exposure has been shown to alter the expression of *Hoxa1* (Stodgell et al., 2006). These reports support the hypothesis that VPA can change the identity of the rhombomeres. In addition, retinoic acid also contributes to the caudalization of the rhombencephalon (Altmann and Brivanlou, 2001; Glover et al., 2006; Yamada, 1994) and alters *Hox* gene expression (Conlon and Rossant, 1992; Langston and Gudas, 1992). Thus, VPA might affect retinoic acid signaling, which in turn regulates *Hox* gene expression.

In chicken embryos exposed to VPA *in ovo*, *Pax6* expression in the eye is diminished (Whitsel et al., 2002), indicating that VPA exposure can alter the expression of *Pax6*. Given that *Pax6* regulates the specification of ventral neuron subtypes in the hindbrain (Takahashi and Osumi, 2002), it is possible that VPA affects the differentiation of facial motor neurons *via Pax6* signaling. These reports indicate that VPA exposure affects the environment in which facial neurons differentiate and migrate within the hindbrain during development.

4.3. Clinical significance

In the present study, exposure of rat embryos to VPA at E9.5 affected the development of the facial nuclei in the hindbrain. In our previous study, we showed that exposure to VPA at E9.5 also affected the development of the peripheral facial nerve (Tashiro et al., 2011). Therefore, VPA exposure at E9.5 affects the development of the entire facial nerve. The embryonic stage E9.5 in rat corresponds to the 3rd week of human gestation. Pregnant women administered VPA, which is used as an anticonvulsant and mood-stabilizing drug, during this stage, sometimes give birth to children with fatal valproate syndrome or autism (Ehlers et al., 1992; Miller et al., 2005). The pharmacokinetic half-life of VPA in humans is 10-fold longer than it is in rodents (Nau et al., 1981), suggesting that the effects of VPA exposure on the development of the facial nerves that we observed in the rat would be more pronounced in humans. Our observations will contribute to the overall understanding of embryonic facial nerve development, and may be used to determine the appropriate conditions for drug administration during pregnancy.

Little is known about the capacity of abnormal morphogenesis during these early stages to cause postnatal physiological dysfunction. In autism patients, disordered caudal migration during the development of the facial nerve nuclei was shown to cause facial disease (Rodier et al., 1996). Analysis of eye-blink in a rat model of autism induced by VPA exposure might help to determine the level of function of the facial nerve. These and future findings may aid in the elucidation of the mechanisms underlying multiple inherent diseases.

Acknowledgments

We thank Thaddeus Dryja for useful comments on this manuscript. This study was supported by the Ministry of Health, Labor and Welfare of the Japanese Government and a Grand-in-Aid from the School of Medicine, Mie University.

References

Altman, J., Bayer, S.A., 1982. Development of the cranial nerve ganglia and related nuclei in the rat. Advances in Anatomy, Embryology and Cell Biology 74, 1–90.
Altmann, C.R., Brivanlou, A.H., 2001. Neural patterning in the vertebrate embryo. International Review of Cytology 203, 447–482.
Bingham, S., Higashijima, S., Okamoto, H., Chandrasekhar, A., 2002. The zebrafish trilobite gene is essential for tangential migration of branchiomotor neurons. Developmental Biology 242, 149–160.
Bloch-Gallego, E., Causeret, F., Ezan, F., Backer, S., Hidalgo-Sánchez, M., 2005. Development of precerebellar nuclei: instructive factors and intracellular mediators in neuronal migration, survival and axon pathfinding. Brain Research. Brain Research Reviews 49, 253–266.
Chandrasekhar, A., 2004. Turning heads: development of vertebrate branchiomotor neurons. Developmental Dynamics 229, 143–161.
Charman, T., Baird, G., 2002. Practitioner review: diagnosis of autism spectrum disorder in 2- and 3-year-old children. Journal of Child Psychology and Psychiatry 43, 289–305.
Chen, P.S., Wang, C.C., Bortner, C.D., Peng, G.S., Wu, X., Pang, H., Lu, R.B., Gean, P.W., Chuang, D.M., Hong, J.S., 2007. Valproic acid and other histone deacetylase inhibitors induce microglial apoptosis and attenuate lipopolysaccharide-induced dopaminergic neurotoxicity. Neuroscience 149, 203–212.
Chédotal, A., Rijli, F.M., 2009. Transcriptional regulation of tangential neuronal migration in the developing forebrain. Current Opinion in Neurobiology 19, 139–145.
Chédotal, A., 2010. Should I stay or should I go? Becoming a granule cell. Trends in Neurosciences 33, 163–172.
Conlon, R.A., Rossant, J., 1992. Exogenous retinoic acid rapidly induces anterior ectopic expression of murine *Hox-2* genes in vivo. Development 116, 357–368.
Ehlers, K., Sturje, H., Merker, H.J., Nau, H., 1992. Valproic acid-induced spina bifida: a mouse model. Teratology 45, 145–154.
Erzurumlu, R.S., Murakami, Y., Rijli, F.M., 2010. Mapping the face in the somatosensory brainstem. Nature Reviews Neuroscience 11, 252–263.
Filipek, P.A., Accardo, P.J., Baranek, G.T., Cook, E.H., Dawson, G., Gordon, B., Gravel, J.S., Johnson, C.P., Kallen, R.J., Levy, S.E., Minshew, N.J., Ozonoff, S., Prizant, B.M., Rapin, I., Rogers, S.J., Stone, W.L., Teplin, S., Tuchman, R.F., Volkmar, F.R., 1999. The screening and diagnosis of autistic spectrum disorders. Journal of Autism and Developmental Disorders 29, 439–484.
Gillberg, C., Winnergård, I., 1984. Childhood psychosis in a case of Moebius syndrome. Neuropediatrics 15, 147–149.
Glover, J.C., Renaud, J.S., Rijli, F.M., 2006. Retinoic acid and hindbrain patterning. Journal of Neurobiology 66, 705–725.
Hatten, M.E., 1999. Central nervous system neuronal migration. Annual Review of Neuroscience 22, 511–539.
Huang, Z., 2009. Molecular regulation of neuronal migration during neocortical development. Molecular and Cellular Neurosciences 42, 11–22.

Ingram, J.L., Peckham, S.M., Tisdale, B., Rodier, P.M., 2000. Prenatal exposure of rats to valproic acid reproduces the cerebellar anomalies associated with autism. Neurotoxicology and Teratology 22, 319–324.
Korematsu, K., Redies, C., 1997. Expression of *cadherin-8* mRNA in the developing mouse central nervous system. Journal of Comparative Neurology 387, 291–306.
Kraus, F., Haenig, B., Kispert, A., 2001. Cloning and expression analysis of the mouse T-box gene *Tbx20*. Mechanisms of Development 100, 87–91.
LaMora, A., Voigt, M.M., 2009. Cranial sensory ganglia neurons require intrinsic N-cadherin function for guidance of afferent fibers to their final targets. Neuroscience 159, 1175–1184.
Langston, A.W., Gudas, L.J., 1992. Identification of a retinoic acid responsive enhancer 3' of the murine homeobox gene *Hox-1.6*. Mechanisms of Development 38, 217–228.
McKay, I.J., Lewis, J., Lumsden, A., 1997. Organization and development of facial motor neurons in the Kreisler mutant mouse. European Journal of Neuroscience 9, 1499–1506.
Meins, M., Henderson, D.J., Bhattacharya, S.S., Sowden, J.C., 2000. Characterization of the human *Tbx20* gene, a new member of the T-box gene family closely related to the Drosophila H15 gene. Genomics 67, 317–332.
Miller, M.T., Strömland, K., Ventura, L., Johansson, M., Bandim, J.M., Gillberg, C., 2005. Autism associated with conditions characterized by developmental errors in early embryogenesis: a mini review. International Journal of Developmental Neuroscience 23, 201–219.
Miyazaki, K., Narita, N., Narita, M., 2005. Maternal administration of thalidomide or valproic acid causes abnormal serotonergic neurons in the offspring: implication for pathogenesis of autism. International Journal of Developmental Neuroscience 23, 287–297.
Narita, M., Oyabu, A., Imura, Y., Kamada, N., Yokoyama, T., Tano, K., Uchida, A., Narita, N., 2010. Nonexploratory movement and behavioral alterations in a thalidomide or valproic acid-induced autism model rat. Neuroscience Research 66, 2–6.
Narita, N., Kato, M., Tazoe, M., Miyazaki, K., Narita, M., Okado, N., 2002. Increased monoamine concentration in the brain and blood of fetal thalidomide- and valproic acid-exposed rat: putative animal models for autism. Pediatric Research 52, 576–579.
Nau, H., Zierer, R., Spielmann, H., Neubert, D., Gansau, C., 1981. A new model for embryotoxicity testing: teratogenicity and pharmacokinetics of valproic acid following constant-rate administration in the mouse using human therapeutic drug and metabolite concentrations. Life Sciences 29, 2803–2814.
Nieto, M.A., Patel, K., Wilkinson, D.G., 1996. In situ hybridization analysis of chick embryos in whole mount and tissue sections. Methods in Cell Biology 51, 219–235.
Noden, D.M., 1993. Spatial integration among cells forming the cranial peripheral nervous system. Journal of Neurobiology 24, 248–261.
Ornitz, E.M., Guthrie, D., Farley, A.H., 1977. The early development of autistic children. Journal of Autism and Childhood Schizophrenia 7, 207–229.
Ornoy, A., 2009. Valproic acid in pregnancy: how much are we endangering the embryo and fetus? Reproductive Toxicology 28, 1–10.
Phiel, C.J., Zhang, F., Huang, E.Y., Guenther, M.G., Lazar, M.A., Klein, P.S., 2001. Histone deacetylase is a direct target of valproic acid, a potent anticonvulsant, mood stabilizer, and teratogen. Journal of Biological Chemistry 276, 36734–36741.
Qu, Y.B., Glasco, D.M., Zhou, L.B., Sawant, A., Ravni, A., Fritzsch, B., Damrau, C., Murdoch, J.N., Evans, S., Pfaff, S.L., Formstone, C., Goffinet, A.M., Chandrasekhar, A., Tissir, F., 2010. Atypical cadherins Celsr1–3 differentially regulate migration of facial branchiomotor neurons in mice. Journal of Neuroscience 30, 9392–9401.
Rodier, P.M., Ingram, J.L., Tisdale, B., Nelson, S., Romano, J., 1996. Embryological origin for autism: developmental anomalies of the cranial nerve motor nuclei. Journal of Comparative Neurology 370, 247–261.
Rodier, P.M., Bryson, S.E., Welch, J.P., 1997. Minor malformations and physical measurements in autism: data from Nova Scotia. Teratology 55, 319–325.
Song, M.R., Shirasaki, R., Cai, C.L., Ruiz, E.C., Evans, S.M., Lee, S.K., Pfaff, S.L., 2006. T-Box transcription factor *Tbx20* regulates a genetic program for cranial motor neuron cell body migration. Development 133, 4945–4955.
Stodgell, C.J., Ingram, J.L., O'Bara, M., Tisdale, B.K., Nau, H., Rodier, P.M., 2006. Induction of the homeotic gene *Hoxa1* through valproic acid's teratogenic mechanism of action. Neurotoxicology and Teratology 28, 617–624.
Strömland, K., Nordin, V., Miller, M., Akerström, B., Gillberg, C., 1994. Autism in thalidomide embryopathy: a population study. Developmental Medicine and Child Neurology 36, 351–356.
Studer, M., Lumsden, A., Ariza-McNaughton, L., Bradley, A., Krumlauf, R., 1996. Altered segmental identity and abnormal migration of motor neurons in mice lacking *Hoxb-1*. Nature 384, 630–634.
Takahashi, M., Osumi, N., 2002. *Pax6* regulates specification of ventral neurone subtypes in the hindbrain by establishing progenitor domains. Development 129, 1327–1338.
Tashiro, Y., Endo, T., Shirasaki, R., Miyahara, M., Heizmann, C.W., Murakami, F., 2000. Afferents of cranial sensory ganglia pathfind to their target inadependent of the site of entry into the hindbrain. Journal of Comparative Neurology 417, 491–500.
Tashiro, Y., Yanagawa, Y., Obata, K., Murakami, F., 2007. Development and migration of GABAergic neurons in the mouse myelencephalon. Journal of Comparative Neurology 503, 260–269.
Tashiro, Y., Oyabu, A., Imura, Y., Uchida, A., Narita, N., Narita, M., 2011. Morphological abnormalities of embryonic cranial nerves after in utero exposure to valproic acid: implications for the pathogenesis of autism with multiple developmental anomalies. International Journal of Developmental Neuroscience 29, 359–364.
Trainor, P.A., Krumlauf, R., 2000. Patterning the cranial neural crest: hindbrain segmentation and *Hox* gene plasticity. Nature Reviews Neuroscience 1, 116–124.
Wada, H., Tanaka, H., Nakayama, S., Iwasaki, M., Okamoto, H., 2006. Frizzled3a and Celsr2 function in the neuroepithelium to regulate migration of facial motor neurons in the developing zebrafish hindbrain. Development 133, 4749–4759.
Whitsel, A.I., Johnson, C.B., Forehand, C.J., 2002. An in ovo chicken model to study the systemic and localized teratogenic effects of valproic acid. Teratology 66, 153–163.
Williams, G., King, J., Cunningham, M., Stephan, M., Kerr, B., Hersh, J.H., 2001. Fetal valproate syndrome and autism: additional evidence of an association. Developmental Medicine and Child Neurology 43, 202–206.
Yamada, T., 1994. Caudalization by the amphibian organizer: brachyury, convergent extension and retinoic acid. Development 120, 3051–3062.
Yamamoto, M., Schwarting, G., 1991. The formation of axonal pathways in developing cranial nerves. Neuroscience Research 11, 229–260.

ELSEVIER

Brain & Development xxx (2012) xxx–xxx

BRAIN & DEVELOPMENT
Official Journal of the Japanese Society of Child Neurology

www.elsevier.com/locate/braindev

Original article

Prenatal exposure to organomercury, thimerosal, persistently impairs the serotonergic and dopaminergic systems in the rat brain: Implications for association with developmental disorders

Michiru Ida-Eto [a,*], Akiko Oyabu [a], Takeshi Ohkawara [a], Yasura Tashiro [a], Naoko Narita [b], Masaaki Narita [a]

[a] *Department of Anatomy II, Mie University Graduate School of Medicine, Tsu, Mie 514-8507, Japan*
[b] *Department of Education, Bunkyo University, Koshigaya, Saitama 343-8511, Japan*

Received 8 November 2011; received in revised form 2 May 2012; accepted 3 May 2012

Abstract

Thimerosal, an organomercury compound, has been widely used as a preservative. Therefore, concerns have been raised about its neurotoxicity. We recently demonstrated perturbation of early serotonergic development by prenatal exposure to thimerosal (Ida-Eto et al. (2011) [11]). Here, we investigated whether prenatal thimerosal exposure causes persistent impairment after birth. Analysis on postnatal day 50 showed significant increase in hippocampal serotonin following thimerosal administration on embryonic day 9. Furthermore, not only serotonin, striatal dopamine was significantly increased. These results indicate that embryonic exposure to thimerosal produces lasting impairment of brain monoaminergic system, and thus every effort should be made to avoid the use of thimerosal.

Keywords: Thimerosal; Serotonin; Dopamine; Embryonic exposure; Developmental disorders; Rat

1. Introduction

Thimerosal, an organomercury compound, has been widely used as a preservative [1]. Thimerosal is metabolized first to ethylmercury and further to inorganic mercury, both of which accumulate in the brain and other organs and have neurotoxic activity [2,3]. Accordingly, use of thimerosal such as vaccines is of great concern, particularly on infants and fetuses [4,5], and therefore, efforts have been made to reduce thimerosal from vaccines [6].

The adverse effects of thimerosal after neonatal administration include impaired pain sensitivity [7], hippocampal neurodegeneration [8], and changes in the dopamine system with subsequent behavioral disorders [9]. In addition, thimerosal was shown to affect neurite extension of neuroblastoma cells *in vitro*, therefore, it is evident that thimerosal leads to neurological abnormalities [10]. However, little is known regarding the prenatal effects of thimerosal. We recently reported that exposure of pregnant rats at gestational day 9 (E9) to thimerosal increased the number of serotonergic neurons in the lateral portion of the caudal raphe in E15 rat hindbrain and thus prenatal thimerosal exposure impaired early serotonergic development [11]. We have also demonstrated that prenatal exposure at E9 to thalidomide or valproic acid (VPA) specifically caused long-term effects on the normal development of serotonergic neuronal systems [12,13], accompanied with behavioral abnormalities that mimicked human

* Corresponding author. Address: Department of Anatomy II, Mie University Graduate School of Medicine, 2-174 Edobashi, Tsu, Mie 514-8507, Japan. Tel.: +81 59 232 1111x6326; fax: +81 59 232 8031.
E-mail address: etom@doc.medic.mie-u.ac.jp (M. Ida-Eto).

0387-7604/$ - see front matter © 2012 The Japanese Society of Child Neurology. Published by Elsevier B.V. All rights reserved.
http://dx.doi.org/10.1016/j.braindev.2012.05.004

Please cite this article in press as: Ida-Eto M et al. Prenatal exposure to organomercury, thimerosal, persistently impairs the serotonergic and dopaminergic systems in the rat brain: Implications for association with developmental disorders. Brain Dev (2012), http://dx.doi.org/10.1016/j.braindev.2012.05.004

autism [14]. Although a relationship between autism and thimerosal has not been confirmed yet [15,16], we need to know whether prenatal thimerosal exposure effects can persist into adulthood. Here, we investigated serotonin and dopamine content in the brains of postnatal day 50 (P50) adult rats following prenatal treatment of thimerosal.

2. Materials and methods

Pregnant Wistar rats were purchased from CLEA Japan, Inc. (Tokyo, Japan). Thimerosal (Sigma–Aldrich, St. Louis, MO) was dissolved in saline, and was administered to pregnant rats on E9 in volume of 50 μl by intramuscular injection into the *glutei maximi*. Thimerosal doses per injection were: 1, 0.1 and 0.01 mg Hg/kg. For the control group, saline was administered in the same manner. Three dams for each group were examined. All animal experiments were authorized by the Animal Research Committee of Mie University.

Measurement of concentration of serotonin (5-HT), dopamine (DA) and their metabolites 5-hydroxyindoleacetic acid (5-HIAA), 3,4-dihydroxyphenylacetic acid (DOPAC) and homovanillic acid (HVA) were performed as described previously [12]. Because brain 5-HT levels are influenced by estrus cycle in females, we used the tissues only from male animals. Each offspring was deeply anesthetized on P50 and then decapitated. The hippocampus and striatum were immediately removed on ice, collected into a tube, frozen with liquid nitrogen, and stored at −80 °C until assay. The tissues were homogenized using an ultrasonic homogenizer (NR-50M; Microtec, Chiba, Japan) in 5 volumes of a mixture of 0.2 M perchloric acid, 100 μM EDTA, and 200 ng of isoproterenol hydrochloride as an internal standard and incubated on ice for 30 min. After centrifugation (20,000*g*, 20 min, 4 °C), the supernatant was adjusted to pH 3 with 1 M sodium acetate and filtered through a 0.45-μm pore size membrane filter (Millex-LH; Millipore, Billerica, MA). A part of the aliquot was separated by high performance liquid chromatography (HPLC) with an electrochemical detector (HTEC-500; Eicom, Kyoto, Japan) and an Eicompak SC-5 ODS column (3.0 mm × 150 mm, Eicom). The mobile phase (0.1 M sodium acetate–citrate acid buffer, pH 3.5, 17% methanol, 190 mg/L sodium 1-octanesulfonate, and 5 mg/L EDTA) allowed for the separation of 5-HT and DA, and their metabolites. Consistent results were obtained from three independent experiments. Statistical evaluation was carried out by grouped *t*-test.

3. Results

To evaluate the potential effects of embryonic exposure to thimerosal on postnatal brain monoamine content, different doses of thimerosal (1, 0.1, and 0.01 mg Hg/kg) were administered to E9 pregnant rats, and then allowed to have pups. When exposed to 1 mg Hg/kg thimerosal, most of the pups were dead soon after birth. On the other hand, in the 0.1 and 0.01 mg Hg/kg thimerosal-exposed groups, no major anomalies, growth retardation, or reduced number of delivered pups were observed in the two groups. Therefore, for monoamine content analysis, thimerosal doses of 0.1 and 0.01 mg Hg/kg were used. Concentrations of hippocampal 5-HT and striatal DA on P50 were measured by HPLC. As shown in the Fig. 1, a significant increase in hippocampal 5-HT levels was observed in the thimerosal-exposed groups (0.01 mg Hg/kg, 266.2 ± 22.2 ng/g weight, $p < 0.05$ vs. control; 0.1 mg Hg/kg, 307.0 ± 7.2 ng/g weight, $p < 0.01$ vs. control; control group, 177.8 ± 27.8 ng/g weight). Striatal DA concentrations were also significantly increased in the exposed groups (0.01 mg Hg/kg, 7039 ± 448 ng/g weight,

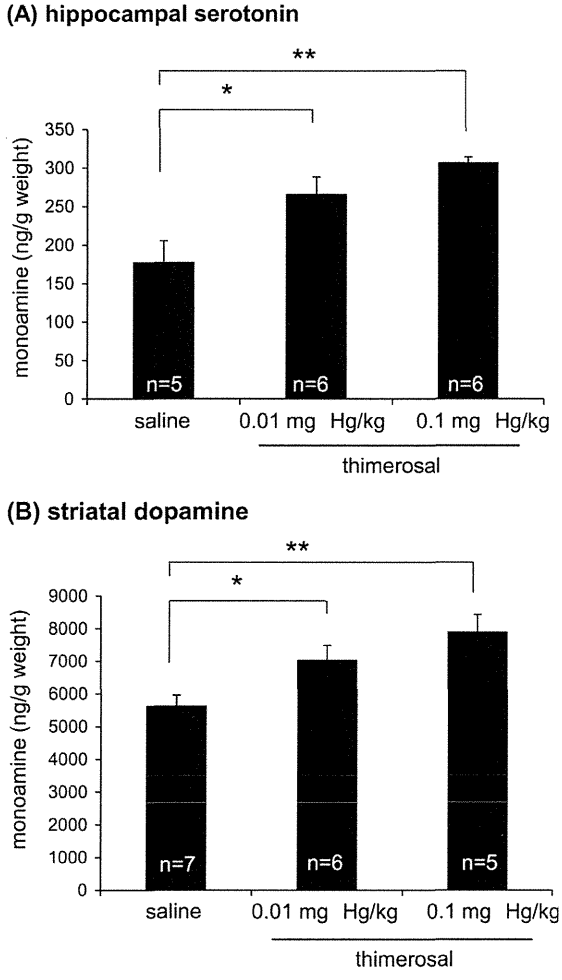

Fig. 1. Monoamine levels in control vs. thimerosal-exposed rats (ng/g weight). Different doses of thimerosal (0.1, and 0.01 mgHg/kg) were administered to E9 pregnant rats, and then allowed to have pups. On P50, concentrations of hippocampal serotonin and striatal dopamine were measured by HPLC. Values are mean ± SEM. $^{*}p < 0.05$ vs. control; $^{**}p < 0.01$ vs. control.

Please cite this article in press as: Ida-Eto M et al. Prenatal exposure to organomercury, thimerosal, persistently impairs the serotonergic and dopaminergic systems in the rat brain: Implications for association with developmental disorders. Brain Dev (2012), http://dx.doi.org/10.1016/j.braindev.2012.05.004

$p < 0.05$ vs. control; 0.1 mg Hg/kg, 7905 ± 520 ng/g weight, $p < 0.01$ vs. control; control group, 5643 ± 323 ng/g weight). Hippocampal 5-HIAA, a metabolite of 5-HT, was also increased in thimerosal-exposed groups compared to control (0.01 mg Hg/kg, 457.8 ± 30.8 ng/g weight, not significant to control; 0.1 mg Hg/kg, 477.4 ± 20.2 ng/g weight, $p < 0.05$ vs. control; control group, 388.2 ± 35.3 ng/g weight), but its increase was not as much as that of 5-HT. Subsequently, the ratio 5-HIAA/5-HT was decreased (control, 2.32 ± 0.26; 0.01 mg Hg/kg, 1.75 ± 0.11, $p < 0.05$ vs. control; 0.1 mg Hg/kg, 1.56 ± 0.06, $p < 0.01$ vs. control). Striatal DOPAC and HVA, a metabolite of DA, was not changed statistically in thimerosal-exposed groups compared to control (0.01 mg Hg/kg, 2082 ± 152 ng/g weight, not significant to control; 0.1 mg Hg/kg, 2225 ± 100 ng/g weight, not significant to control; control group, 1997 ± 103 ng/g weight). The ratio (DOPAC + HVA)/DA was also decreased (control, 0.356 ± 0.011; 0.01 mg Hg/kg, 0.295 ± 0.007, $p < 0.01$ vs. control; 0.1 mg Hg/kg, 0.283 ± 0.010, $p < 0.01$ vs. control). These results indicate that prenatal exposure to thimerosal on E9 affects levels of 5-HT and DA, and their metabolites in the adult brain.

4. Discussion

In this study, we demonstrated that prenatal exposure to thimerosal on E9 caused a significant increase in 5-HT and DA content in the brains of adult rats. This finding indicates that prenatal thimerosal exposure may cause lasting neurochemical impairments to the serotonergic and dopaminergic systems.

Prenatal exposure to thimerosal has been shown to alter early embryonic development of 5-HT in our previous study [11]. These findings, together with those of the present study, suggest that a single prenatal exposure to thimerosal causes irreversible and critical effects to the brain serotonergic system. Persistent effects caused by a single prenatal exposure to chemicals are not, however, surprising because we have previously reported that prenatal exposure on E9 to thalidomide or VPA, chemicals known to induce autism when exposed at E9 [17,18], also induced increased hippocampal 5-HT in the adult brains of rats at P50 [12,13]. In thalidomide or VPA experiments, behavioral abnormalities in rats closely mimicked human autism [14]. Importantly, we also showed that abnormalities in 5-HT content caused by prenatal thalidomide exposure were time-specific (i.e., on E9). Therefore, the present result that exposure to thimerosal on E9 caused 5-HT abnormalities is consistent with previous findings. Because the possible link between thimerosal and autism is still controversial [15,16], further experiments are necessary to resolve this issue.

Prenatal exposure to thimerosal also seems to cause persistent changes in the striatal dopaminergic neuron of the brain. Faro et al. demonstrated that ethylmercury and methylmercury increased the *in vivo* release of DA from the striatum in free-moving adult rats [19]. Olczak et al. demonstrated that early postnatal administration of thimerosal caused persistent changes of the dopamine system in rats [9]. Therefore, mercury can cause short- and long-term effects on the dopaminergic system. However, to the best of our knowledge, our present report is the first to demonstrate that the effects from prenatal exposure to thimerosal persisted through the P50 dopaminergic and serotonergic systems. Because both dopaminergic and serotonergic neurons are known to be fated to develop from precursors starting from about E9, with help from the sonic hedgehog and fibroblast growth factor 8 genes [20], exposure to thimerosal at E9 is thought to cause irreversible effects on serotonergic and dopaminergic neurons. Further experiments are necessary to determine how thimerosal perturbs the normal development of both neurons.

Hippocampal 5-HIAA, a metabolite of 5-HT, were also increased in thimerosal-exposed groups compared to control, but its increase was not as much as that of 5-HT. Subsequently, the ratio 5-HIAA/5-HT was apparently decreased. Striatal (DOPAC + HVA)/DA ratio was decreased. We are not sure whether this decreased ratio means the true change of neurotransmitter metabolism, i.e., change of monoamine oxidase (MAO) level. However, in any case, the fact that thimerosal-dependent increase of 5-HT was more or less accompanied by 5-HIAA increase and that thimerosal-dependent increase of DA suggests that fetal exposure to thimerosal causes somehow lasting change of neurotransmitter metabolism. Further study to lead the conclusion of the effects of thimerosal on neurotransmitter metabolism such as by analyzing MAO activity will be published elsewhere.

Acknowledgment

This study was supported in part by the Ministry of Health, Labour and Welfare of the Japanese Government.

References

[1] Magos L. Review on the toxicity of ethylmercury, including its presence as a preservative in biological and pharmaceutical products. J Appl Toxicol 2001;21:1–5.
[2] Clarkson TW, Magos L. The toxicology of mercury and its chemical compounds. Crit Rev Toxicol 2006;36:609–62.
[3] Dórea JG. Integrating experimental (*in vitro* and *in vivo*) neurotoxicity studies of low-dose thimerosal relevant to vaccines. Neurochem Res 2011;36:927–38.

Please cite this article in press as: Ida-Eto M et al. Prenatal exposure to organomercury, thimerosal, persistently impairs the serotonergic and dopaminergic systems in the rat brain: Implications for association with developmental disorders. Brain Dev (2012), http://dx.doi.org/10.1016/j.braindev.2012.05.004

[4] Ball LK, Ball R, Pratt RD. An assessment of thimerosal use in childhood vaccines. Pediatrics 2001;107:1147–54.
[5] Young HA, Geier DA, Geier MR. Thimerosal exposure in infants and neurodevelopmental disorders: an assessment of computerized medical records in the Vaccine Safety Datalink. J Neurol Sci 2008;271:110–8.
[6] Verstraeten T, Davis RL, DeStefano F, Lieu TA, Rhodes PH, Black SB, et al. Safety of thimerosal-containing vaccines: a two-phased study of computerized health maintenance organization databases. Pediatrics 2003;112:1039–48.
[7] Olczak M, Duszczyk M, Mierzejewski P, Majewska MD. Neonatal administration of a vaccine preservative, thimerosal, produces lasting impairment of nociception and apparent activation of opioid system in rats. Brain Res 2009;1301:143–51.
[8] Olczak M, Duszczyk M, Mierzejewski P, Bobrowicz T, Majewska MD. Neonatal administration of thimerosal causes persistent changes in mu opioid receptors in the rat brain. Neurochem Res 2010;35:1840–7.
[9] Olczak M, Duszczyk M, Mierzejewski P, Meyza K, Majewska MD. Persistent behavioral impairments and alterations of brain dopamine system after early postnatal administration of thimerosal in rats. Behav Brain Res 2011;223:107–18.
[10] Lawton M, Iqbal M, Kontovraki M, Lloyd Mills C, Hargreaves AJ. Reduced tubulin tyrosination as an early marker of mercury toxicity in differentiating N2a cells. Toxicol In Vitro 2007;21:1258–61.
[11] Ida-Eto M, Oyabu A, Ohkawara T, Tashiro Y, Narita N, Narita M. Embryonic exposure to thimerosal, an organomercury compound, causes abnormal early development of serotonergic neurons. Neurosci Lett 2011;505:61–4.
[12] Narita N, Kato M, Tazoe M, Miyazaki K, Narita M, Okado N. Increased monoamine concentration in the brain and blood of fetal thalidomide- and valproic acid-exposed rat: putative animal models for autism. Pediatr Res 2002;52:576–9.
[13] Miyazaki K, Narita N, Narita M. Maternal administration of thalidomide or valproic acid causes abnormal serotonergic neurons in the offspring: implication for pathogenesis of autism. Int J Dev Neurosci 2005;23:287–97.
[14] Narita M, Oyabu A, Imura Y, Kamada N, Yokoyama T, Tano K, et al. Nonexploratory movement and behavioral alterations in a thalidomide or valproic acid-induced autism model rat. Neurosci Res 2010;66:2–6.
[15] Thompson WW, Price C, Goodson B, Shay DK, Benson P, Hinrichsen VL, et al. Early thimerosal exposure and neuropsychological outcomes at 7 to 10 years. N Engl J Med 2007;357:1281–92.
[16] Price CS, Thompson WW, Goodson B, Weintraub ES, Croen LA, Hinrichsen VL, et al. Prenatal and infant exposure to Thimerosal from vaccines and immunoglobulins and risk of autism. Pediatrics 2010;126:656–64.
[17] Strömland K, Nordin V, Miller M, Akerström B, Gillberg C. Autism in thalidomide embryopathy: a population study. Dev Med Child Neurol 1994;36:351–6.
[18] Williams G, King J, Cunningham M, Stephan M, Kerr B, Hersh JH. Fetal valproate syndrome and autism: additional evidence of an association. Dev Med Child Neurol 2001;43:202–6.
[19] Faro LR, Rodrigues KJ, Santana MB, Vidal L, Alfonso M, Durán R. Comparative effects of organic and inorganic mercury on *in vivo* dopamine release in freely moving rats. Braz J Med Biol Res 2007;40:1361–5.
[20] Ye W, Shimamura K, Rubenstein JLR, Hynes MA, Rosenthal A. FGF and Shh signals control dopaminergic and serotonergic cell fate in anterior neural plate. Cell 1998;93:755–66.

Please cite this article in press as: Ida-Eto M et al. Prenatal exposure to organomercury, thimerosal, persistently impairs the serotonergic and dopaminergic systems in the rat brain: Implications for association with developmental disorders. Brain Dev (2012), http://dx.doi.org/10.1016/j.braindev.2012.05.004

Acta Histochemica xxx (2012) xxx–xxx

Contents lists available at SciVerse ScienceDirect

Acta Histochemica

journal homepage: www.elsevier.de/acthis

Short communication

Subtype-specific parafollicular localization of the neuropeptide manserin in the rat thyroid gland

Takeshi Ohkawara[a,*], Akiko Oyabu[a], Michiru Ida-Eto[a], Yasura Tashiro[a], Naoko Narita[b], Masaaki Narita[a]

[a] Department of Developmental and Regenerative Medicine, Mie University, Graduate School of Medicine, Mie, Japan
[b] Department of Education, Bunkyo University, Saitama, Japan

ARTICLE INFO

Article history:
Received 16 March 2012
Received in revised form 2 April 2012
Accepted 9 May 2012
Available online xxx

Keywords:
Manserin
Thyroid gland
Parafollicular cell
Follicular epithelial cell
Neuropeptide
Chromogranin
Secretogranin

ABSTRACT

The thyroid gland is an endocrine organ which is involved in metabolism, neuroexcitability, body growth and development. The thyroid gland is also involved in the regulation of calcium metabolism, which is not yet fully understood. In this study, we investigated the localization of the granin-derived neuropeptide, manserin, in the adult rat thyroid gland. Manserin immunoreactivity was detected in thyroid follicular epithelial cells. Intense manserin signals were also detected in some, but not all, parafollicular cells, indicating that parafollicular manserin may be subtype-specific. These results indicate that thyroid manserin may play pivotal roles in parafollicular cells and follicular epithelial cells such as in calcium metabolism and/or thyroid hormone secretion.

Introduction

The thyroid gland plays an important role in the body by promoting metabolism, increasing neuroexcitability, accelerating body growth and development, and increasing cardiac function (Cheng et al., 2010). The thyroid gland is also involved in the regulation of calcium metabolism. A protein called thyroglobulin is secreted by thyroid follicular epithelial cells into the lumen of thyroid follicles. After iodination, thyroglobulin is again taken up by the follicular epithelial cells (Spitzweg et al., 2000). The hormones thyroxine (T4) and triiodothyronine (T3) are then released (internally secreted) into the circulation (Spitzweg et al., 2000).

Parafollicular cells of the thyroid gland are known to be involved in regulating serum Ca^{2+} levels through calcitonin secretion. Only one parafollicular cell type is known to date. However, the existence of somatostatin-positive and somatostatin-negative subtypes of parafollicular cells has been proposed (Sawicki and Zabel, 1997), suggesting that parafollicular cells may be heterogeneous. However, the precise morphological and functional distinctions among parafollicular cells have still not been elucidated.

We recently isolated manserin, a neuropeptide composed of 40 amino acids, by combining HPLC and affinity purification (Yajima et al., 2004). Manserin is distributed in the rat pituitary, hypothalamic nuclei, adrenal gland, duodenum epithelial cells, cerebellum, inner ear, and β and δ cells in the pancreatic islets (Yajima et al., 2004, 2008; Kamada et al., 2010; Tano et al., 2010; Ohkawara et al., 2011; Ida-Eto et al., 2012), indicating that manserin plays roles in several endocrine systems. Manserin has not previously been found in the thyroid gland. However, the fact that SgII, a manserin precursor, occurs in thyroid parafollicular cells (Weiler et al., 1989; Schmid et al., 1992) suggests that manserin might also occur in the thyroid gland. Because SgII is reported to have Ca^{2+}-binding ability (Yoo et al., 2007), manserin is also expected to have some roles in Ca^{2+} metabolism. In addition, parafollicular cells secrete numerous regulatory peptides that play important roles in their functions (Sawicki, 1995). For these reasons, we sought to identify the localization of manserin in the adult thyroid gland.

Materials and methods

Animals

Four male Wistar rats (8–12 weeks old) were used. All animal experiments were approved by the Committee of Laboratory Animal Research Center at Mie University.

* Corresponding author at: Department of Developmental and Regenerative Medicine, Mie University, Graduate School of Medicine, 2-174 Edobashi, Tsu, Mie 514-8507, Japan.
E-mail address: tohkawara@doc.medic.mie-u.ac.jp (T. Ohkawara).

0065-1281/$ – see front matter © 2012 Elsevier GmbH. All rights reserved.
http://dx.doi.org/10.1016/j.acthis.2012.05.003

Please cite this article in press as: Ohkawara T, et al. Subtype-specific parafollicular localization of the neuropeptide manserin in the rat thyroid gland. Acta Histochemica (2012), http://dx.doi.org/10.1016/j.acthis.2012.05.003